Available online at www.sciencedirect.com
SCIENCE DIRECT®
Journal of Organometallic Chemistry 684 (2003) 124–143
Journal of Organometallic Chemistry
www.elsevier.com/locate/jorganchem

Mechanism of copper(I)-catalyzed cyclopropanation: a DFT study calibrated with copper(I) alkene complexes

Bernd F. Straub [a,b], Irene Gruber [a], Frank Rominger [a], Peter Hofmann [a,*]

[a] Organisch-Chemisches Institut der Universität Heidelberg, Im Neuenheimer Feld 270, D-69120 Heidelberg, Germany
[b] Department Chemie, Ludwigs-Maximilians-Universität München, Butenandtstr. 5-13 (Haus F), D-81377 Munchen, Germany

Received 26 March 2003; received in revised form 16 May 2003; accepted 16 May 2003

Dedicated to Professor Ernst Otto Fischer on the occasion of his 85th birthday

Abstract

The complete catalytic cycle of copper-catalyzed cyclopropanation is investigated by density functional model calculations. The study focuses on obtaining accurate relative stabilities of the ligand–metal cores of all catalytic intermediates and transition states. The copper iminophosphanamide $[H_2P(NH_2)_2-\kappa^2N]Cu$ serves as model fragment, since three copper catalyst key intermediates with an iminophosphanamide ligand have been isolated or detected. The electronic structure of the active intermediates, copper(I) carbenes of the d^{10}-ML_3 type, and their reactivity towards ethene and vinyl alcohol is investigated. The reliability of the computed data is confirmed by their comparison with experimental data of $[t\text{-}Bu_2P(NSiMe_3)_2-\kappa^2N]Cu$ alkene and alkyne complexes, using relative ligand binding strengths and alkene ligand rotation barriers. The uncharged nature of the model complexes minimizes solvation artifacts and thus renders the evaluation of associative and dissociative ligand exchange pathways possible. The associative alkene ligand exchange with diazoalkane to a $\kappa N,\kappa O$-diazoalkane complex, subsequent intramolecular rearrangement to a κC-complex and N_2 extrusion are identified on the most probable pathway to the electrophilic copper(I) carbene complexes of the Fischer type. They are predicted to react with alkenes to labile cupracyclobutanes with a planar $N_2Cu^{III}C_2$ core, which undergo facile reductive elimination of a cyclopropane derivative.

Keywords: Homogeneous catalysis; Carbene ligands; N ligands; Copper; Density functional calculations; Cyclopropanation; Copper carbenes

1. Introduction

The mechanism of copper-catalyzed cyclopropanation of alkenes by α-carbonyl diazoalkanes has been of considerable interest for more than 35 years [1,2]. Nozaki et al. successfully applied the copper-catalyzed cyclopropanation reaction as the first enantioselective homogeneous transition metal catalysis [2]. Initially, copper(II) carbene species of the d^9-ML_5 type were assumed to be the cyclopropanating species [1]. However, the importance of copper(I) in the catalytic cycle was verified by Aratani [3] and the Pfaltz co-workers [4]. Copper(II) complexes are inactive and have to be reduced in situ e.g. by addition of hydrazine or by heating with the diazoalkane substrate [3,4]. The role and structure of cupracyclobutanes were unclear [3]. Pfaltz rationalized the origin of the excellent enantioselectivities obtained with C_2-symmetrically substituted bidentate nitrogen ligands such as semicorrins. The different steric repulsion of the acyl substituent at the carbene with bulky groups of the spectator ligand in the diastereomeric transition states is in accordance with the observed enantioselectivities [4]. Kinetic investigations by the group of Pérez ascertained the presence of a preequilibrium before the rate-determining N_2 loss of the diazoalkane [5]. Copper(I) alkene complexes are the resting states of the catalytic cycle [6,7]. Until 2000, they were the only isolated or detected intermediates.

The synthesis of copper(I) alkene iminophosphanamide precursor complexes **1** and **2** [8] made possible the isolation of a sterically stabilized copper diazoalkane

* Corresponding author. Tel.: +49-6221-54-8502; fax: +49-6221-54-4885.
E-mail address: ph@phindigo.oci.uni-heidelberg.de (P. Hofmann).

0022-328X/03/$ - see front matter © 2003 Elsevier B.V. All rights reserved.
doi:10.1016/S0022-328X(03)00520-5

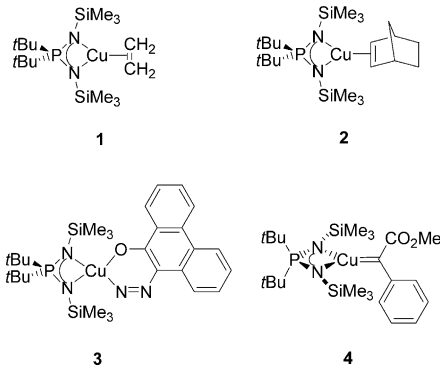

Fig. 1. Copper iminophosphanamide complexes **1**–**4**.

complex **3** [9] and the detection of a reactive copper(I) carbene species **4** (Fig. 1) [10]. This copper carbene iminophosphanamide complex of the d^{10}-ML_3 type has been identified experimentally as the active species in the cyclopropanation reaction.

The experimental progress towards unravelling the mechanism of copper-catalyzed cyclopropanation [5,8–10] has been accompanied by quantum-chemical investigations [11–14]. Recent theoretical studies by others on cationic copper model systems are left with the uncertainty of energetic consequences of solvation and counterion effects [12–14]. Here we focus on obtaining reliable model energies by the use of simplified models, such as **5**–**8**, of experimentally characterized species **1**–**4**, thus benefiting from minimal solvation artifacts due to the uncharged nature of these iminophosphanamide complexes (Fig. 2).

Our strategy here is to ensure the reliability of computed energy barriers within the catalytic cycle by comparison of experimental alkene rotation barriers in solution and relative alkene copper binding strengths with quantum-chemical gas phase data of the analogous simplified copper iminophosphanamide systems.

As a model for α-carbonyl diazoalkanes such as methyl-2-phenyl-2-diazoacetate [10], 2-diazoethanal is used. We are well aware that the steric demand of *t*-butyl, trimethylsilyl, phenyl, methoxy and benzo groups may result in slower intermolecular reactions and intramolecular rearrangements. Thus, we want to focus on the inherent reactivity of the copper iminophosphanamide fragment towards models of these substrates, which are actually present in cyclopropanation reactions.

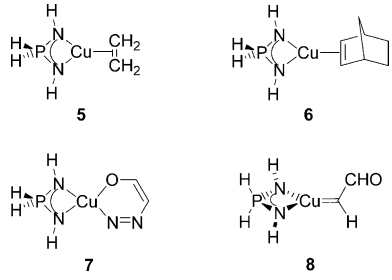

Fig. 2. Simplified model complexes **5**–**8**.

2. Computational methods

For all DFT calculations, the empirically parametrized B3LYP method [15] within the GAUSSIAN-98 package was used [16]. The geometry optimizations and vibrational frequency analyses were performed using the Stuttgart/Dresden (SDD) multielectron-fit 19 valence electron effective core potential and basis set for Cu [17] and the 6-31G(d) basis set for C, N, P, O and H [18]. In addition, geometry optimizations and vibrational frequency analyses were also performed with the 6-31G(d) basis set on all atoms.

All equilibrium structures have been characterized by the lack of imaginary vibrations, and transition states have been characterized by the presence of exactly one imaginary vibration.

The SDD ECP and basis set with an additional diffuse ($\alpha_f = 0.24$) and an additional compact polarization *f* function ($\alpha_f = 3.70$) for Cu [17,19] and the 6-311+G(2d,p) basis set [20] for C, N, P, O and H were used for single-point energy calculations and NBO analyses [21] of structures optimized with the SDD/6-31G(d) basis set. Single-point energies and NBO analyses were also determined with the 6-311+G(2d,p) basis set for the structures optimized with the 6-31G(d) basis set. The energies obtained with the latter method are given in parentheses unless otherwise noted.

The single-point electronic energies were corrected to free Gibbs energies at 298.15 K and 1 atm based on the unscaled harmonic frequencies obtained with the [SDD/6-31G(d)] or 6-31G(d) basis sets.

The quasirelativistic character of the SDD ECP should not be of importance in copper chemistry, in contrast to the chemistry of the heavier congeners silver and in particular gold [22]. However, the SDD basis set possesses a valence shell of triple-ζ quality. Geometries and energies of interactions of copper with ligand atoms should significantly benefit from this feature.

3. Discussion and results

First, we want to report new copper(I) iminophosphanamide complexes. Their structures, their intramolecular degenerate rearrangements and their ligand exchange equilibria are tailor-made for the verification of the suitability of the level of theory applied here.

3.1. Syntheses and structures of copper(I) alkene and alkyne complexes

The copper(I) maleic anhydride complex **9**, the 1,4-benzoquinone complex **10** and the styrene complex **11** were synthesized in one-pot procedures (Scheme 1). This synthetic pathway has already been reported by us for the ethene and norbornene analogue [8].

The maleic anhydride complex **9** has been fully characterized, including a single crystal X-ray diffraction study (Fig. 3).

The dimethyl butynedioate ligand easily replaces ethene in the corresponding complex **1**, yielding the alkyne complex **12** (Scheme 2). This high affinity for copper(I) will be further discussed in Sections 3.3 and 3.5.

In the solid state (Fig. 4), the C≡C bond length of the alkyne ligand in complex **12** remains very short (1.236(4) Å), indicating weak copper to alkyne backbonding.

3.2. Alkene ligand rotation barriers

We have already reported the intramolecular degenerate rotation barrier of the norbornene ligand in complex **6** [8]. Due to the local C_{2v} symmetry of the iminophosphanamide copper(I) moiety and the lower C_s symmetry of the copper alkene fragment, the ^{1}H- and ^{13}C{^{1}H}-NMR signals of the *t*-Bu groups display temperature-dependent behavior. Determination of the coalescence temperature gives access to the Gibbs free activation energy of the responsible molecular rearrangement (Scheme 3).

The coalescence of the pseudotriplet/quartet signal of the *t*-Bu protons to a doublet in the maleic anhydride complex **9** can be observed by VT-^{1}H-NMR spectroscopy (Fig. 5).

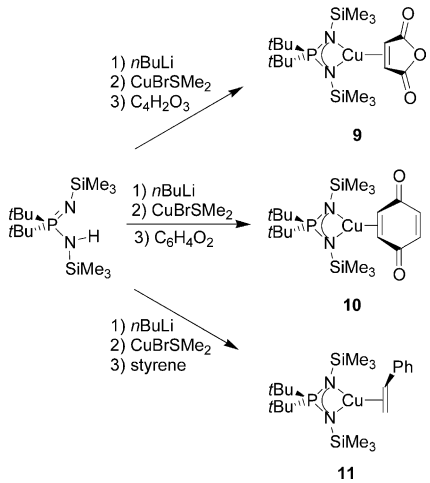

Scheme 1. Syntheses of copper(I) alkene iminophosphanamide complexes.

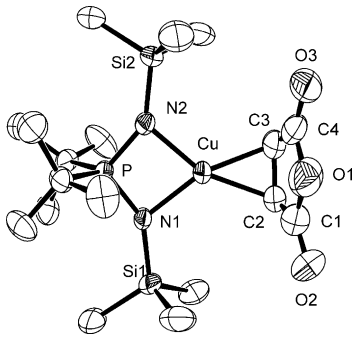

Fig. 3. Molecular structure of **9** in the solid state. Hydrogens of the iminophosphanamide ligand are omitted for clarity. Thermal ellipsoids are drawn at the 50% probability level. Average values of the three independent molecules with assumed C_s-symmetry in the unit cell (averaged non-crystallographic standard deviation): bond lengths (Å) P–N 1.613(5), Si–N 1.717(7), Cu–N 1.966(10), Cu–C 2.005(25), C1–C2 1.435(44), C2–C3 1.430(52), C1–O1 1.409(18), C1–O2 1.193(23). Bond angles (°) P–N1–Si1 146.9(1.6), N1–P–N2 102.2(6), P–N–Cu 89.1(4), N1–Cu–N2 79.4(3). Dihedral angles (°) N1–P–N2–Cu 2.1(2.4), N1–Cu–C2–C3 174.2(6.0).

In ^{13}C{^{1}H}-NMR spectra of complex **9** at different temperatures, both the coalescence of the two doublets of the diastereotopic quarternary *t*-Bu carbon atoms to one doublet and the coalescence of the two singlets of the *t*-Bu methyl carbons to one singlet are observed (Fig. 6).

Comparable coalescence phenomena for the P*t*-Bu$_2$ unit in the ^{1}H-NMR spectra were also observed for the 1,4-benzoquinone and styrene complexes **10** ($\Delta G^{\ddagger} = 48.5$ kJ mol^{-1}) and **11** ($\Delta G^{\ddagger} = 37.0$ kJ mol^{-1}). The C_1 symmetry of the copper styrene moiety is the origin of the additional non-equivalence of the trimethylsilyl groups in the ground state geometry. The coalescence temperature of the carbon and proton NMR signals of the trimethylsilyl groups was also measured in this case.

In the 1,4-benzoquinone complex **10**, an additional fluxional process and an intermolecular equilibrium are active. Kläui co-workers has already reported these processes for a copper(I) benzoquinone complex with a tridentate ancillary ligand [23]. In their system, a coalescence temperature of about 305 K corresponds to a Gibbs free activation barrier of about 60 kJ mol^{-1} for the exchange of the coordinated and the non-coordinated alkene site of the 1,4-benzoquinone ligand. In our benzoquinone system **10**, a Gibbs free activation energy of 49.7 kJ mol^{-1} is derived from the ^{1}H-NMR spectra shown in Fig. 7. The higher barrier in the Kläui system can be rationalized by the necessity to break one coordinative bond of the ancillary ligand in order to

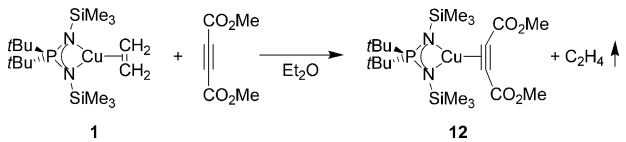

Scheme 2. Synthesis of alkyne complex **12**.

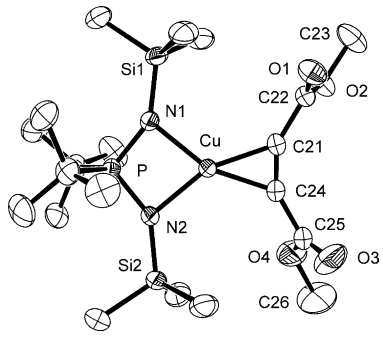

Fig. 4. Molecular structure of [t-Bu$_2$P(NSiMe$_3$)$_2$–κ^2N]Cu[η^2-C$_2$(CO$_2$Me)$_2$] **12** in the solid state. Thermal ellipsoids are drawn at the 50% probability level. Hydrogen atoms are omitted for clarity. Bond lengths (Å) P–N 1.611(2) and 1.615(2), Si–N 1.710(2) and 1.711(2), Cu–N 1.979(2) and 1.983(2), Cu–C 1.922(3) and 1.929(3), C21–C24 1.236(4), C21–C22 1.482(4), C24–C25 1.485(4), C22–O1 1.18(1), C25–O3 1.17(1), C22–O2 1.329(4), C25–O4 1.330(6), O2–C23 1.453(4), O4–C26 1.468(5). Bond angles (°) P–N–Si 146.3(1) and 147.5(1), N1–P–N2 102.1(1), P–N–Cu 89.5(1) and 89.8(1), N1–Cu–N2 78.6(1), C21–C24–C25 149.9(3). Dihedral angle (°) N1–P–N2–Cu 0.1.

avoid a 20 valence electron copper(I) species in the η^4-benzoquinone transition state.

The presence of a dinuclear μ-benzoquinone complex **13** and free benzoquinone accounts for the small signals in the ^{1}H-NMR spectrum in Fig. 7. Since they do not participate in the coalescence of the signals of the mononuclear complex **10**, intermolecular alkene site exchange reactions via dinuclear species such as **13** possess comparably high Gibbs free activation energies.

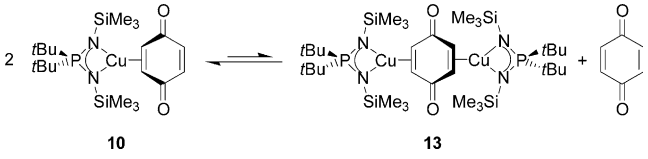

Scheme 5. Equilibrium of mononuclear complex **10** with dinuclear complex **13** and 1,4-benzoquinone.

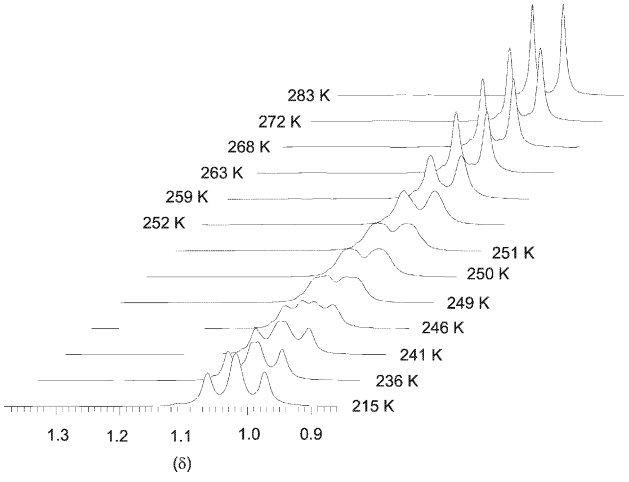

Fig. 5. ^{1}H-NMR spectra of **9** in toluene-d_8 at 300.13 MHz: coalescence

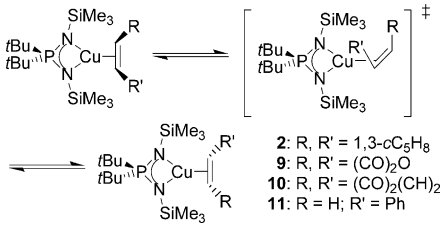

Scheme 3. Topology of the intramolecular degenerate alkene ligand rotation in complexes **2**, **9**, **10** and **11**.

Thus, the observed facile alkene site exchange has to proceed intramolecularly via **10b**‡ (Scheme 5).

The alkene site exchange in complex **10** (Scheme 4 and Fig. 7), however, will also lead to a coalescence of t-butyl NMR signals. Since the t-Bu coalescence phenomena and the alkene site exchange coalescence require similar Gibbs activation barriers, the barrier of the 1,4-benzoquinone ligand rotation has to be at least 48.5 kJ mol^{-1}, as derived from the ^{1}H and ^{13}C{^{1}H}-NMR coalescence measurements of the t-Bu groups.

3.3. Relative ligand bond strengths

Relative stabilities of copper(I) alkene iminophosphanamide complexes were derived by integration of ^{1}H-NMR signals. Solutions of copper(I) alkene complexes were mixed with a different free alkene. The resulting equilibria contain four species: two free alkenes and two copper(I) alkene complexes. The integrals of the alkene proton signals were normalized with respect to the number of protons in the alkene. The Gibbs free energy differences ΔG were derived from the equilibrium constants K in Eq. (1).

$$\Delta G = -RT \ln K \quad (1)$$

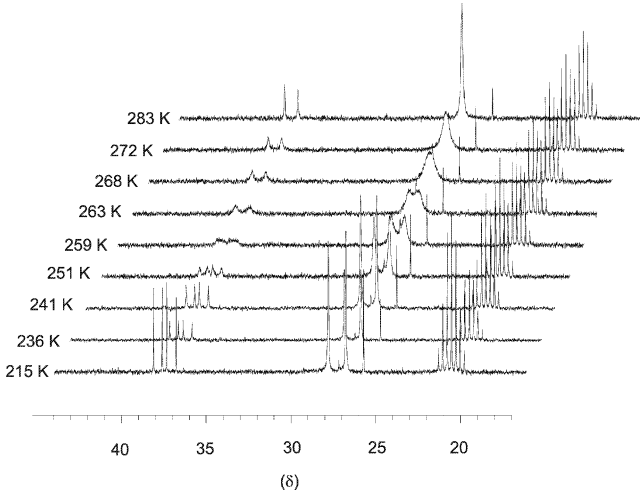

Fig. 6. ^{13}C{^{1}H}-NMR spectra of **9** in toluene-d_8 at 75.47 MHz: coalescence phenomena of the signals of the quaternary carbons of t-butyl groups and of the methyl singlets, respectively. The septet at δ = 20.4 is the carbon signal of the CD$_3$ group of the toluene-d_8 solvent.

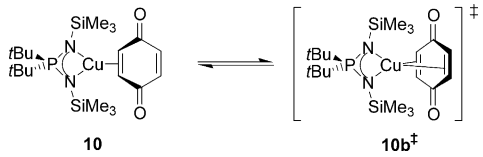

Scheme 4. Alkene site exchange via a η^4-1,4-benzoquinone transition state.

The ethene complex **1** plus norbornene is about (4±2) kJ mol^{-1} less stable than norbornene complex **2** plus ethene. The maleic anhydride complex **9** is (13.6±3) kJ mol^{-1} less stable than norbornene complex **2**. Accordingly, benzoquinone complex **10** is (12.2±3) kJ mol^{-1} less stable than complex **2**. Dimethyl butynedioate complex **12** can be quantitatively synthesized from ethene complex **1** and free alkyne ligand. Ethene is rapidly evolved even at 1 bar external pressure, indicating a much higher relative thermodynamic stability of the dimethyl butynedioate complex. For a comparison of quantum-chemically derived binding energies and experimentally observed relative copper alkene bond strengths, see Section 3.5 and Tables 2 and 3.

3.4. Benefit of uncharged model complexes

Computed relative gas phase energies of ionic complexes can differ significantly from the experimental relative energies of the complexes in solution. The coordination strength of ligands to cationic metal fragments in the gas phase is larger than in solution, since the positive charge is stabilized by the larger available molecular volume. Additionally, donor solvents will be able to coordinate to the metal center itself. This point is of considerable importance for copper cyclopropanation catalysts, since they are mostly cationic. Association and dissociation reactions are particularly sensitive towards these solvation effects. Furthermore, even weakly coordinating counterions can bind to copper(I) complexes [24]. Cationic copper complexes with achiral spectator ligands and an enantiopure chiral counterion were actually shown to yield enantioenriched cyclopropanes [25]. Thus, uncharged models such as the copper(I) iminophosphanamide system provide the chance to minimize solvation artifacts when comparing computed gas phase energies with experimental chemistry in hydrocarbon solutions. For neutral systems, a deviation of the computed relative free energies of model systems in the gas phase from solution chemistry data of less than 20 kJ mol^{-1} thus appears to be possible. This is supported by the comparison of predicted and observed degenerate rearrangement barriers for the norbornene complex **2** and its model **6** and for the diazoalkane complex **3** and its model **7** [8,9].

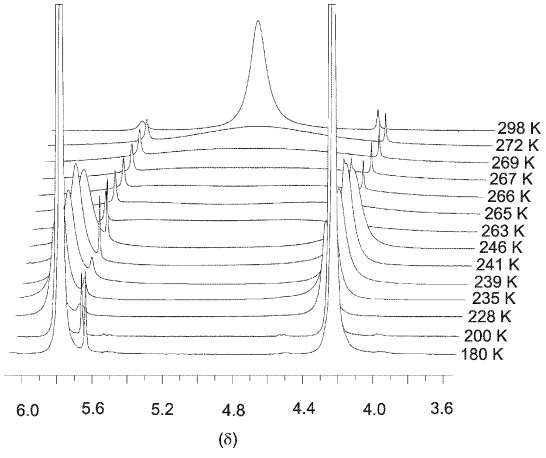

Fig. 7. ^{1}H-NMR spectra of **10** in toluene-d_8 at 300.13 MHz: coalescence phenomenon of the singlets of the non-coordinated and coordinated alkene protons of the 1,4-benzoquinone ligand; additional traces of free 1,4-benzoquinone at low field and presumably of a dicopper(I) μ-benzoquinone complex **13** at high field.

3.5. Comparison of theory and experiment: calibration of computational data

The reliability of computed energies is of major importance for the quantitative discussion of a catalytic reaction pathway.

The accuracy of computed relative energies of model complexes compared to experimental data generally suffers from several limitations. In order to ensure only small energetic deviations between reality and theory for hypothetical intermediates and transition states, we compare experimental barriers of degenerate rearrangements with their computed DFT model counterparts. Furthermore, experimental and quantum-chemically derived relative bond strengths of alkene ligands to copper(I) are compared.

Previously, we have confirmed the reliability of the B3LYP/6-311+G(2d,p)//B3LYP/6-31G(d) level of theory in Cu^I/Cu^{III} chemistry by the good agreement of structural parameters, relative energies, degenerate rearrangement barriers and IR frequencies for the diazoalkane complex **3** and the computed data of its simplified model $[H_2P(NH_2)_2{-}\kappa^2N]Cu[OC_2H_2N_2{-}\kappa O,\kappa N]$ **7** [9].

The degenerate rotation of the norbornene ligand in copper(I) complex **2** with a free Gibbs energy of activation of $\Delta G^{\ddagger}_{199K} = 41.5$ kJ mol^{-1} [8] provides a further test of the reliability of the quantum-chemical methodology. The free Gibbs energy of activation of the model complex **6** (Fig. 8) is computed to 23.9 kJ mol^{-1} (27.4 kJ mol^{-1}).

Essentially, the rotational barrier parallels the difference of the backbonding strength of the N_2Cu moiety towards a coplanar or orthogonal alkene. The underrating of the rotation barrier of about 12–18 kJ mol^{-1} indicates that the structural simplifications and the level

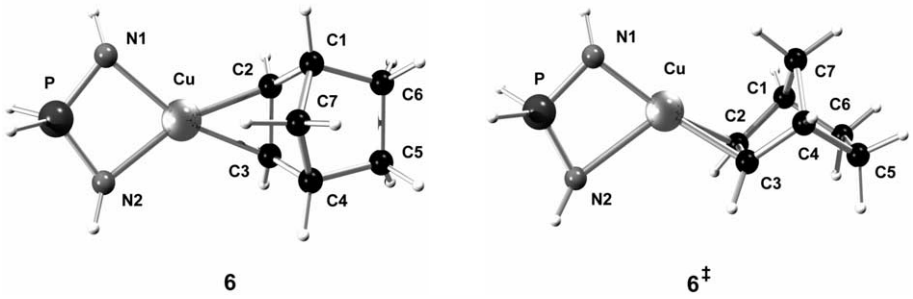

Fig. 8. Ball-and-stick models of norbornene complex **6** and transition state **6**‡. Relevant bond lengths for **6**: d(Cu–N1) = d(Cu–N2) = 2.053 Å; d(Cu–C2) = d(Cu–C3) = 2.036 Å; d(C2–C3) = 1.398 Å. Relevant bond distances for **6**‡: d(Cu–N1) = 1.931 Å; d(Cu–N2) = 2.396 Å; d(Cu–C2) = 2.091 Å; d(Cu–C3) = 2.082 Å; d(C2–C3) = 1.383 Å.

of theory lead to an underestimation of the backbonding capability of the copper fragment.

In the model system, the iminophosphanamide ligand displays an interesting feature: the nitrogens of the [$H_2P(NH)_2$–κ^2N]Cu model systems are pyramidalized ($130^\circ < \delta(\mathrm{NPNH}) < 140^\circ$), in contrast to the nearly planar nitrogen substituent environment in the real [t-$Bu_2P(NSiMe_3)_2$–κ^2N]Cu complexes. As a consequence, two diastereomers e.g. for carbene model complex **8** with a free Gibbs energy difference of 0.4 kJ mol^{-1} (0.8 kJ mol^{-1}) were found. No efforts were made to calculate the diastereomers of all models relevant in the computed reactions, since the energy differences of the diastereomers should also be very small and irrelevant for the experimental system with its trimethylsilyl groups and planarized nitrogen binding environment.

We performed further calibrations using the alkene rotation in the copper maleic anhydride complex **9** and 1,4-benzoquinone iminophosphanamide complex **10** and the intramolecular alkene site exchange in the latter [11a]. Furthermore, we compared the alkene and alkyne copper(I) binding energies of the complexes **5**, **6**, **14**, **15** and **16** (Fig. 9) with the relative binding capabilities of their experimental counterparts **1**, **2**, **9**, **10** and **12**.

The data of both the experimental NMR investigations as well as the quantum-chemical data for the simplified model complexes is depicted in Table 1.

The quantum-chemical model prediction of alkene ligand rotation barriers is consistently underestimated.

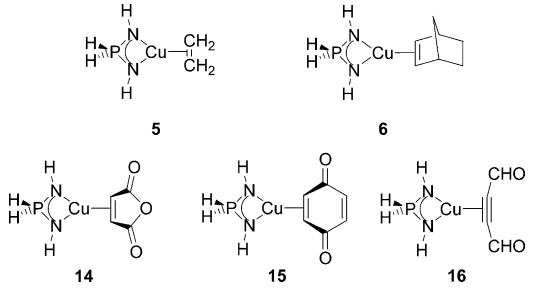

Fig. 9. Computed copper(I) alkene model complexes.

The backbonding capability of copper(I) computed for our model systems appears to be too low, which might also result in somewhat destabilized copper(III) model species at this level of theory.

The experimental Gibbs free energy difference of (4 ± 2) kJ mol^{-1} between ethene complex **1** plus norbornene and norbornene complex **2** plus ethene is perfectly reflected in the computed energy difference of the ethene model complex **5** and the norbornene model complex **6** at triple-ζ basis set levels of theory (Tables 2 and 3). The complexes **14** and **15** are computed to be the least stable model complexes, again in accordance with experiment. Therefore, the qualitative ligand to metal strength ordering is correctly reproduced by the used level of theory. The quantitative comparison between experiment and theory is accurate within 10 kJ mol^{-1}, which is very satisfactory for an isodesmic reaction involving a transition metal.

All comparisons of experimental and computed data emphasize that systematic errors at the present level of theory, solvation and electronic effects of the t-butyl and trimethylsilyl groups result in deviations of relative energies of computed models from experimental data of less than 20 kJ mol^{-1}. Therefore, the following model calculations for catalytic cyclopropanation should reflect reality in a reasonable fashion.

3.6. Mechanism of copper-catalyzed cyclopropanation

A complete cycle of copper-catalyzed cyclopropanation is described. Various reaction pathways of a copper(I) ethene iminophosphanamide model complex with 2-diazoethanal yielding a copper(I) carbene species are evaluated. The electronic structure of copper carbenes of the d^{10}-ML_3 type is characterized. Their intrinsic reactivity towards alkenes and the stability of cupracyclobutanes are of major interest for the understanding of the origin of enantioselectivities and diastereoselectivities with enantiopure chiral chelating N-ligands.

Table 1
Comparison of experimental Gibbs free activation energies of **11**, **2**, **10** and **9** with calculated ligand rotation barriers of model complexes **6**, **15** and **14**

Gibbs free rotation energy barriers for [Cu]–L in (kJ mol^{-1})	Experimental	Quantum-chemical model prediction	Difference
L = styrene	37.0±2.0 (**11**)	–	–
L = norbornene	41.5±2.0 (**2**)	23.9 (26.0) (**6**)	17.6 (15.5)
L = 1,4-benzoquinone (intramolecular alkene site exchange)	>48.5 (**10**)	36.0 (36.3) (**15**)	>12.5(>12.2)
	49.7±2.0	49.0 (47.4)	0.7 (2.3)
L = maleic anhydride	53.7±2.0 (**9**)	40.5 (41.3) (**14**)	13.2 (12.4)

3.6.1. Preequilibrium

Copper(I) alkene complexes are the resting states of the catalytic cycle of copper-catalyzed cyclopropanation [6,7]. In the computed carbene complex formation pathway (Fig. 10), the ethene model complex **5** is indeed the most stable species before the rate-determining N_2 loss via transition state **23**. Copper diazoalkane model complex **7** is more stable than its isomers **20** and **22** (Figs. 10–12). Thus, the $\kappa N,\kappa O$ coordination mode of α-carbonyl diazoalkanes is the most favored for copper iminophosphanamides. Indeed, the diazoalkane complex **3** has been isolated and structurally characterized [9]. The steric inhibition of the N_2 extrusion pathway and the thermodynamic stabilization due to the pronounced diazoniophenolate character of the diazophenanthrone ligand are responsible for the unusual stability of **3** [9]. The existence of a preequilibrium involving copper alkene complexes is reflected in the rate-retarding effect of high alkene concentrations in cyclopropanation catalysis [5,9]. Experimentally, an equilibrium of ethene complex **1**, diazoalkane, free ethene and diazoalkane complex **3** has been confirmed [9].

3.6.2. Associative versus dissociative ligand exchange

The reactivity of α-carbonyl diazoalkanes could be at least in part due to the role of the oxo functionality as ligand atom in the copper carbene formation pathway. The question whether the alkene diazoalkane ligand exchange is associative or dissociative, is not relevant for the explanation of the existence of a preequilibrium. Nonetheless, the comparison of alternative pathways would increase the general understanding of copper(I) reaction mechanisms. Two associative and the dissociative alkene diazoalkane ligand exchange mechanisms were investigated in order to find the lowest-energy pathway (Fig. 10).

In the first associative ligand replacement reaction, the diazoalkane complex **7** can be formed from ethene complex **5** and N_2CHCHO via transition state **17**. The second associative ethene diazoalkane exchange via transition state **18** leads directly to the κ^1C-diazoalkane complex **22**. In a dissociative pathway, the liberated 14 valence electron copper fragment coordinates to the diazoalkane, yielding either one of the diazoalkane complex isomers **7**, **20** or **22**.

The formation of diazoalkane complex **7** can only be of relevance for cyclopropanation, if a facile intramolecular rearrangement pathway to diazoalkane complex **22** is accessible, from which N_2 is liberated. The rearrangement of diazoalkane complex **7** to the η^2-carbonyl model complex **20** and subsequently to the copper(I) κ^1C diazoalkane complex **22** is indeed predicted to be facile.

The Gibbs ethene ligand dissociation energy in **5** is computed to be 86.1 (75.1) kJ mol^{-1}, which is very similar to the barrier for the associative exchange via **17** (Figs. 10 and 11 and Table 4). However, the theoretical underestimation of the backbonding capability of copper(I) of 12–18 kJ mol^{-1} derived in Section 3.5 from the rotation barriers in copper(I) alkene complexes indicates that real copper alkene bond strengths could well be somewhat higher than computed. Since the Gibbs free energy of transition state **18** is predicted to be higher than that of **17**, the $\kappa N,\kappa O$ exchange via **17** with a subsequent rearrangement pathway appears to be the most probable route for copper carbene complex formation. The possibility of an intramolecular rearran-

Table 2
Computed copper alkene dissociation energies of model complexes **5**, **6**, **14**, **15** and **16**

	5	**6**	**14**	**15**	**16**
6-31G(d)	141.1 (250.2)	131.1 (264.5)	123.0 (264.7)	123.8 (260.8)	136.3 (276.8)
Zero point correction	8.7 (10.8)	5.2 (7.5)	6.6 (7.9)	6.2 (7.4)	5.8 (6.8)
6-311+G(2d,p)	140.2 (133.5)	138.4 (132.5)	131.6 (128.4)	132.9 (128.8)	143.2 (139.6)
6-311+G(2d,p) zero point corrected	131.5 (122.7)	133.2 (125.0)	125.0 (120.5)	126.7 (121.4)	137.4 (132.8)
BDE (298.15 K, 1 atm)	134.0 (125.6)	132.9 (125.4)	125.5 (121.1)	126.9 (121.7)	137.5 (133.1)

Energies in (kJ mol^{-1}).

Table 3
Observed relative copper alkene bond strengths of complexes **1**, **2**, **9**, **10** and **12**

	1	**2**	**9**	**10**	**12**
Relative Gibbs free energies at ambient conditions, accuracy 2–3 kJ mol^{-1}	11.6	13.6	1.4	0	$\gg$11.6

Energies in (kJ mol^{-1}).

gement pathway to κ^1C-diazoalkane complexes has been previously analyzed by us [9]. In a computational study on cationic copper species, $\kappa N,\kappa O$-diazoalkane complexes such as **3** were assumed to be only intermediates in an unproductive side-equilibrium [13]. However, the competing pathways were not considered in this study.

In the present work, the dissociative and one of the two associative pathways come out with too similar free activation barriers to make reliable general predictions for copper(I) systems, in particular for cationic catalysts. Increased steric demand of substituents in real systems will inevitably lead to a destabilization of transition states for associative ligand exchange reactions, while the positive charge in cationic copper complexes should favor associative pathways with a tetracoordinated copper center. In the gas phase, a copper ethene diazoalkane complex analogous to structure **18** has been computed to be only 27.2 kJ mol^{-1} higher in Gibbs free energy than free diazoalkane and a copper(I) ethene N,N'-dimethyl malonaldiimine cation [13].

Long-range interactions of the copper center with the diazo or carbonyl group appear to be only reproducible with diffuse basis functions on copper. For transition state **19** and diazoalkane complex **22** (Figs. 10 and 12), the SDD ECP and basis set on copper have a distinct stabilizing effect. For **22**, a weak coordination of the carbonyl group was obtained in the B3LYP/6-31G(d) geometry optimization. With the Stuttgart–Dresden basis set on copper, only the coordination of the diazo carbon was found. Complex **22** is classified as a d^{10}-ML$_3$ type complex with an approximate Y-shape coordina-

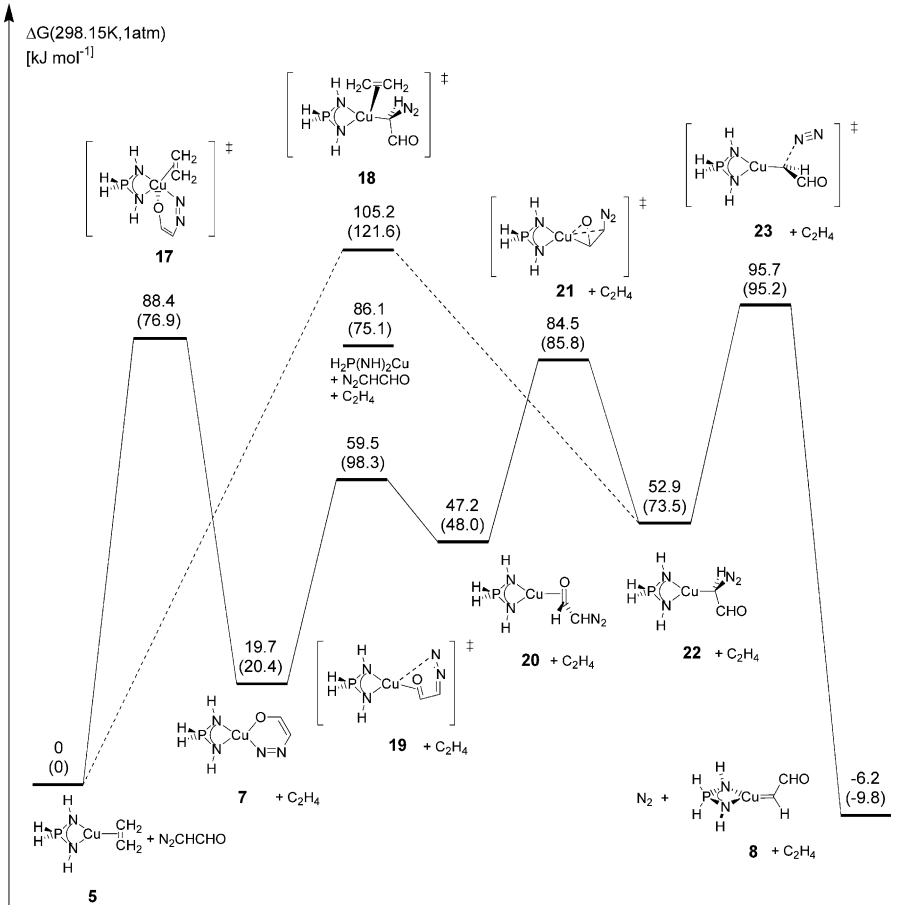

Fig. 10. Computed formation pathway of copper(I) carbene model complex **8** from ethene complex **5**. Gibbs free energies refer to B3LYP/SSD*+,6-311+G(2d,p)//B3LYP/SDD,6-31G(d) (in parentheses B3LYP/6-311+G(2d,p)//B3LYP/6-31G(d)).

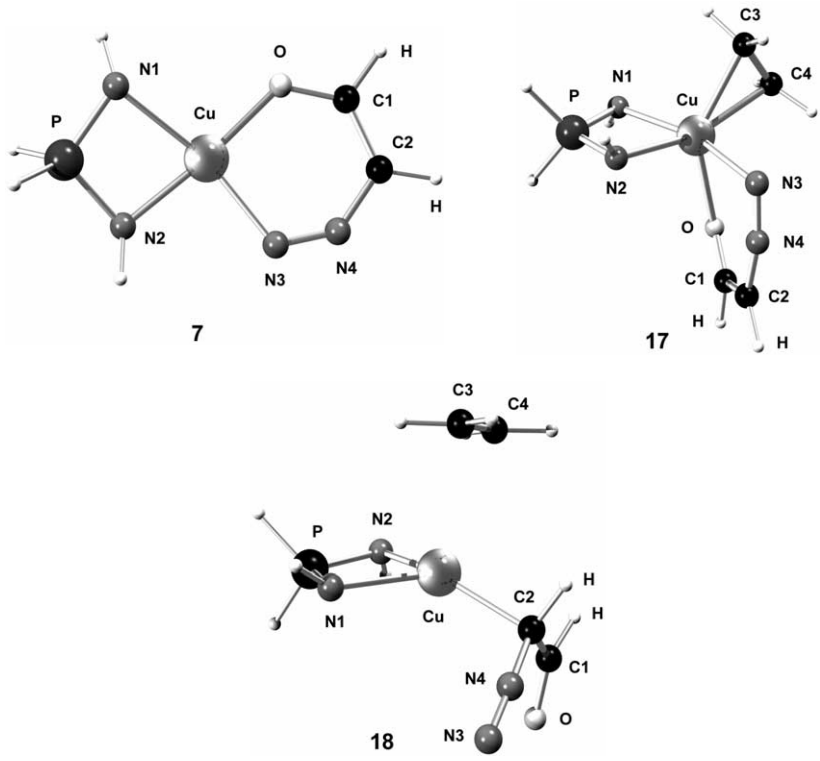

Fig. 11. Ball-and-stick models of diazoalkane complex **7** and the transition states **17** and **18** for the computed associative ethene diazoalkane ligand exchange.

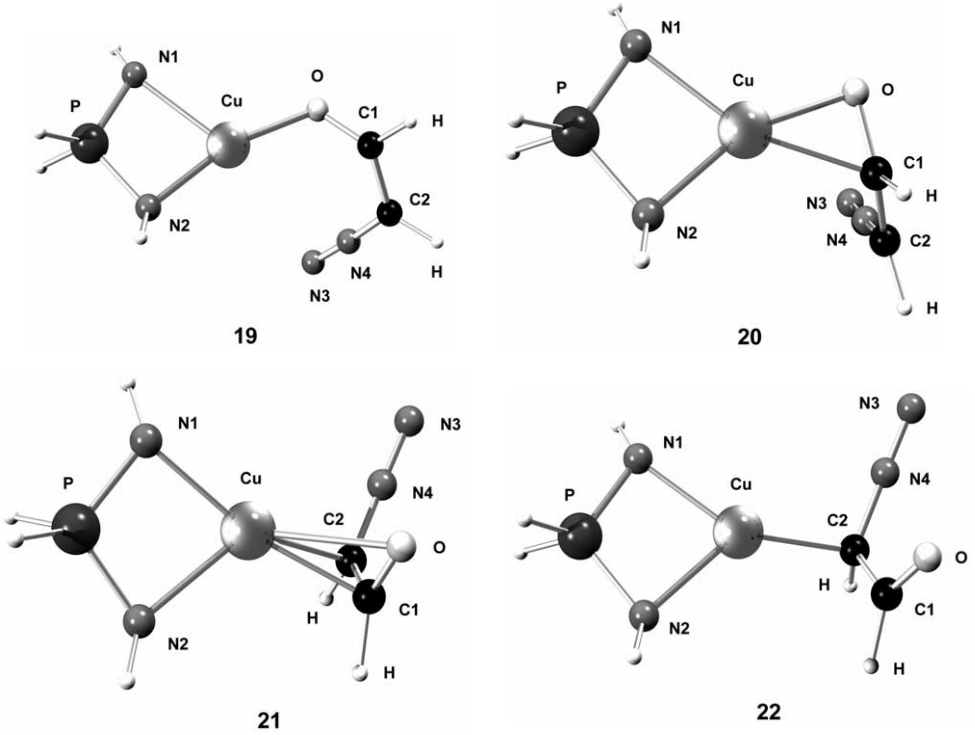

Fig. 12. Ball-and-stick models of the transition state **19** for the η^2-carbonyl model complex **20**, η^3-transition state **21** and the $\kappa^1 C$ diazoalkane complex **22**.

Table 4
Relevant bond lengths (Å) of the copper iminophosphanamide complexes **7**, **8** and **17**–**23** [B3LYP/{SDD/6-31G(d)}]

	7	**8**	**17**	**18**	**19**	**20**	**21**	**22**	**23**
d(Cu–N1)	2.134	2.012	2.264	2.115	2.248	2.095	2.014	2.038	2.070
d(Cu–N2)	1.973	2.023	2.036	2.079	1.962	1.991	2.094	2.096	2.037
d(Cu–N3)	1.987	–	2.373	3.586	3.766	4.208	3.791	3.598	3.696
d(Cu–C1)	2.850	2.923	3.112	2.725	2.753	2.162	2.079	2.723	2.831
d(Cu–C2)	3.256	1.794	3.488	2.069	3.489	3.081	2.290	2.010	1.866
d(Cu–C3)	–	–	2.131	2.790	–	–	–	–	–
d(Cu–C4)	–	–	2.125	2.759	–	–	–	–	–
d(Cu–O)	1.914	3.582	2.209	3.455	1.935	1.920	2.391	3.478	3.643
d(O–C1)	1.266	1.218	1.240	1.215	1.251	1.277	1.245	1.213	1.214
d(C1–C2)	1.394	1.464	1.430	1.488	1.428	1.455	1.471	1.494	1.475
d(C2–N4)	1.358	–	1.328	1.353	1.322	1.313	1.325	1.360	1.778
d(N3–N4)	1.187	–	1.152	1.126	1.132	1.137	1.133	1.126	1.117
d(C3–C4)	–	–	1.367	1.340	–	–	–	–	–

tion geometry of the copper center (α(N–Cu–C) = 137.0° and 146.5°). The dative bond of the κ^1C diazoalkane ligand leads to a diazonio type $RN^+{\equiv}N$ group (*d*(N–N) = 1.126 Å). Previous classifications of κ^1C diazoalkane species as copper(III) complexes (T shape, d^8-ML_3 type) [14] are difficult to rationalize in this context.

3.6.3. Carbene complex formation

The N_2 extrusion via transition state **23** has the highest overall free Gibbs energy of activation of the computed catalytic cycle (Figs. 10 and 13). The diazo carbon in **23** needs a high backbonding capability of the copper fragment in order to electronically stabilize the empty p orbital of the carbene carbon. Accordingly, copper complexes with π-acids such as phosphanes are only suited as precatalysts for α-carbonyl diazoalkane decomposition and cyclopropanation reactions. They have to lose phosphane in order to yield catalytically active species. The effective depopulation of the copper d^{10} shell by π-acidic ligands reduces the backbonding strength to other ligands and thus hampers the formation of the strongly π-acidic carbene ligand from the σ-donor κC-diazoalkane ligand. Induction periods are required for phosphane dissociation and the formation of catalytically active copper(I) species. It is thus understandable that experimentally hard bidentate or tridentate σ- and π-donor nitrogen ligands are best suited to yield electron-rich copper(I) fragments with a high backbonding capability and stability towards disproportionation to metallic copper and copper(II).

The most important structural data of the model complexes of the cyclopropanation cycle are shown in Table 4.

3.6.4. Structure of copper carbenes

The copper carbon bond length in **8** is computed to be 1.794 Å, which is significantly shorter than in thiazole derived carbene copper complexes in the solid state (1.868(6) and 1.888(6) Å) [26] and in MP2 calculations of Wanzlick–Arduengo carbene copper complexes (1.84–1.87 Å) [27]. The Cu–C bond is comparable to the previously computed 1.782 Å in a cationic copper carbene model complex [14]. The orthogonality of the carbene moiety and the PN_2Cu fragment in the copper(I) carbene complex **4** has been unambiguously ascertained in a previous report, since the *t*-butyl substituents at the phosphorus are diastereotopic at the NMR time scale at room temperature [10]. In accordance with this observation, the carbene model

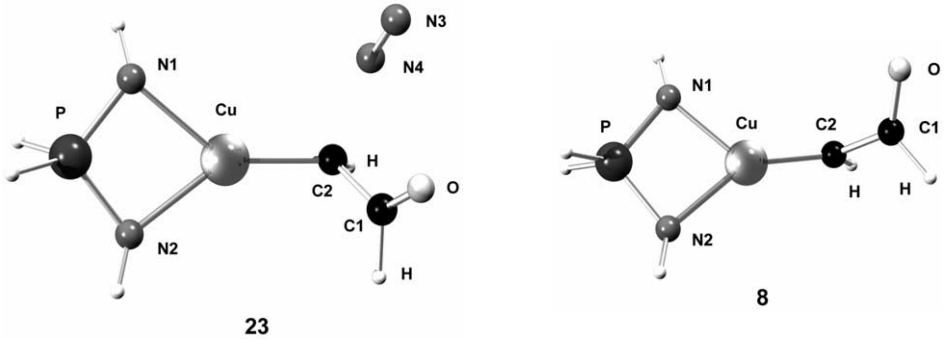

Fig. 13. Ball-and-stick models of the transition state for N_2 extrusion **23** and carbene complex **8**.

complex **8** has nearly orthogonal carbene and PN_2Cu fragments. Carbene complex **8**, N_2 and C_2H_4 have a slightly negative free Gibbs energy of formation from ethene complex **5** and 2-diazoethanal. From a purely electronic point of view, the carbene complex formation is disfavored by 54.5 kJ mol^{-1} (49.9 kJ mol^{-1}). The large difference between electronic and free Gibbs energies is mainly due to the entropically favored N_2 formation. Nevertheless, copper(I) fragments are excellent leaving groups, both from a kinetic and from a thermodynamic point of view. In accordance with the exergonic carbene model complex formation, the experimental preparation of the parent complex **4** in a steady-state concentration from ethene complex **1** and methyl-2-phenyl-2-diazoacetate has been successful [10]. In the real system **4**, the mesomeric stabilization of the electrophilic carbene by a phenyl substituent further favors the formation of the carbene complex.

An NBO analysis of **8** reveals that copper(I) carbene complexes of the d^{10}-ML_3 type possess a true copper carbon double bond. The π-bond is mainly localized at the copper fragment (74.6%) with 9.5% s and 90.4% d character. The carbene carbon contributes mainly by its p orbital (95.7%). The σ-bond is a dative bond of the lone pair of the singlet carbene fragment (82.6% carbon character with 30.9% s and 69.1% p contribution) to the copper fragment (17.4% copper character with 12.7% d and 87.0% s contribution). The carbene carbon is sp^2 hybridized (CH bond 32.3% s and 67.6% p; CC bond 32.7% s and 67.0% p).

The asymmetry of the carbene fragment induces a distortion of the Y-shape of the ideal d^{10}-ML_3 geometry and subsequently leads to sd mixing at the copper center. This intrafragment polarisation is also the origin of the significant copper s character in the π-bond. The facile sd mixing of copper and the facile sp mixing at the carbene carbon rationalize the fact of symmetry-allowed [2+2] addition reactions of alkenes with copper carbenes of the d^{10}-ML_3 type.

An ab initio study of Böhme and Frenking has confirmed that the copper carbon bond in copper complexes of Wanzlick–Arduengo carbenes, which have weak or no π acceptor character has only little backbonding character [27]. The low π-acidity of Wanzlick–Arduengo–Öfele carbene ligands has been shown in Ref. [28]. However, copper carbenes of the d^{10}-ML_3 type such as **4** or model **8** possess a much stronger copper carbon π-interaction.

In summary, copper(I) carbene complexes such as **4** or **8** should be classified as Fischer [29] carbenes. The designation of the active species in copper-catalyzed cyclopropanation as copper carbenoids, however, is misleading. Copper 'carbenoids' do not only react as if they were carbene complexes; they are carbene complexes.

3.6.5. Isomers of carbene complexes

Due to the capability of the carbonyl group to coordinate to the copper center, isomers of the carbene complex **8** are possible. Indeed, a copper(III) model complex **24** with nearly coplanar PN_2Cu and CuC_2O moieties is a local minimum (Figs. 14 and 15). Model **24** is less stable by $\Delta G = 16.3$ kJ mol^{-1} (17.1 kJ mol^{-1}) than the carbene complex **8**. A phenyl substituent at the carbene as in the experimental complex **4** should further mesomerically stabilize the carbene complex. Additionally, a cupraoxacyclobutene analogous to **24** would be destabilized by the steric repulsion of the trimethylsilyl groups with the phenyl substituent compared to the experimental carbene complex **4**. This is in accordance with the free Gibbs energy of activation of $\Delta G^{\ddagger} > 60$ kJ mol^{-1} for carbene rotation in the carbene complex **4** [10].

Interestingly, the free Gibbs energy difference at the B3LYP/6-31G(d) level of theory favors copper(III) model **24** with its higher copper coordination number by 10.6 kJ mol^{-1}, while the B3LYP/[SDD/6-31G(d)] methodology predicts carbene complex **8** to be more stable by 20.1 kJ mol^{-1}—in accordance with the relative single-point energies obtained with the more flexible basis sets. Thus, the accurate prediction of energies of some copper species and even the shape of energy surfaces may significantly depend on the quality of the basis set on copper. A triple-ζ quality basis set on copper seems to be mandatory for a reasonable computational treatment of some copper species. Similar basis set effects may also be relevant for the quantum-chemical study of similar species in other copper-catalyzed reactions such as the aziridination of alkenes by PhI=NTs [30,31].

3.6.6. Analogies to aziridination

The isolobality of acyl carbene and sulfonyl nitrene ligands has led to the assumption that analogous nitrene complexes could be the active species in copper-catalyzed aziridination of alkenes. In a DFT study with triple-ζ plus polarization quality basis set on copper, Gillespie et al. have only found copper complexes **A** with a monodentate nitrene ligand (Fig. 16) [30]. In contrast, Brandt et al. found bidentate κ*N*, κ*O* sulfonyl nitrene structures **B** throughout [31]. For geometry optimization, they used a double-ζ quality basis set without polarization or diffuse functions on copper. Even though different spectator ligands were used in these

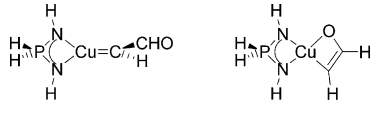

8 **24**

Fig. 14. Copper(I) carbene model complex **8** and isomeric copper(III) vinyl alcoholate derivative **24**.

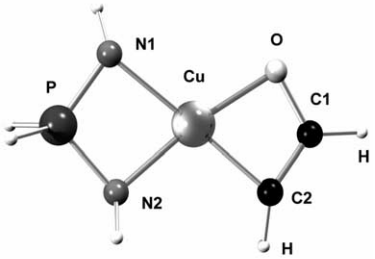

24

Fig. 15. Ball-and-stick models of the copper(III) complex **24**. Relevant computed bond lengths and angles for **24**: d(Cu–N1) = 2.058 Å; d(Cu–N2) = 1.929 Å; d(Cu–O) = 1.892 Å; d(Cu–C2) = 1.931 Å; d(C1–C2) = 1.345 Å; d(C1–O) = 1.341 Å; α(N1–Cu–N2) = 77.5°; α(C2–Cu–O) = 70.4°.

studies, the contrasting findings indicate that analogous basis set effects could also be present in copper nitrene chemistry.

3.6.7. Carbene ligand rotation

The rotation barriers of carbene and alkene ligands around CuN_2 fragments reflect the strength of the backbonding character. Such data is of relevance for the detailed understanding of the copper carbon double bond.

The intrinsic barrier for carbene rotation at an N_2Cu fragment is difficult to derive from data of an acyl substituted carbene model complex such as **8**. The possibility of oxygen coordination to the copper center and formation of copper(III) complexes such as **24** interferes with the rotation of the carbene. Thus, the rotation of a methylene ligand in model complex **25** was investigated (Figs. 17 and 18).

A transition state **26** for the rotation of the methylene group is found to lie 35.9 kJ mol^{-1} (37.1 kJ mol^{-1}) higher in energy than equilibrium structure **25** (Fig. 17). The C_2-symmetric structure **27** is only a third-order [SDD/6-31G(d)] or a second-order stationary point [6-31G(d)] with a 48.5 kJ mol^{-1} (47.7 kJ mol^{-1}) higher free Gibbs energy. The methylene rotation barrier is significantly lower than the experimental lower limit of 60 kJ mol^{-1} for carbene ligand rotation in complex **4** [10]. However, an analogous underestimation of the electronic ligand rotation barrier as in the norbornene model complex **6** is probable. Furthermore, the steric demand of the [t-Bu$_2$P(NSiMe$_3$)$_2$–κ^2N]$^-$ ligand system should contribute to the destabilization of the coplanar carbene coordination mode in the real carbene complex **4**.

The small N–Cu–N bite angle in copper iminophosphanamides results in a particularly high backbonding capability of the copper center [8], which strengthens the π-bond to the methylene group. Upon rotation of the methylene ligand, the capto-dative stabilization of the four-membered PN_2Cu cycle disappears, and the ring strain results in the formation of a carbene complex **26** of the d^{10}-ML$_2$ type comparable to the copper(I) complexes previously reported with Wanzlick–Arduengo carbene ligands [26]. The CuC bond length of 1.788 Å in **25** increases to 1.795 Å in **26**, although the coordination number of copper decreases. In **27**, the copper carbon distance of 1.806 Å is again slightly larger.

Due to the flat energy surface, sterically demanding substituents at the iminophosphanamide ancillary ligand may well lead to a ground state with a geometry such as in stationary point **27** (Fig. 18 and Table 5).

3.6.8. Cyclopropanation

The C–C bond formation reaction from carbene complex **8** to the copper complex **29** is highly exergonic, reflecting the weakness of the copper carbene double bond compared to carbon–carbon bonds (Fig. 19).

In complex **29**, one of the two carbon–carbon bonds has already been formed. The highly delocalized species **29** can either be viewed as a copper(I) complex with strong back-donation into a cyclopropane C–C σ* molecular orbital and the π* orbital of the carbonyl moiety, or as an ylidic 4-cupronio(III)-1-buten-1-olate with an intramolecular coordination of the partial carbon–carbon double bond. The Gibbs free energy of activation via transition state **28** of 54.8 kJ mol^{-1} (59.0 kJ mol^{-1}) has no inherent electronic origin, since the electronic barrier only amounts to 3.8 kJ mol^{-1} (4.8 kJ mol^{-1}). Zero point corrections and entropic contributions result in this significant difference between $\Delta E^{\ddagger}_{tot}$ and $\Delta G^{\ddagger}$.

An alkene with an electron-donating substituent such as vinyl alcohol as a model of enol ethers has an even lower Gibbs free activation energy for the C–C bond formation reaction. Transition state **33** has a 43.4 kJ mol^{-1} (43.6 kJ mol^{-1}) higher Gibbs free energy than carbene complex **8** and vinyl alcohol (Fig. 20). The high reactivity of electron-rich alkenes in copper-catalyzed

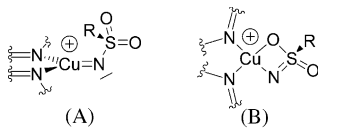

Fig. 16. Proposed monodentate and κN, κO sulfonyl nitrene intermediates in copper-catalyzed aziridination of alkenes [30,31].

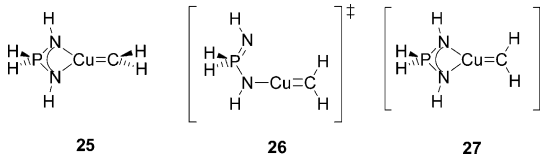

Fig. 17. Copper(I) carbene model complex **25**, transition state **26** for carbene rotation and C_2-symmetrical higher-order stationary point **27**.

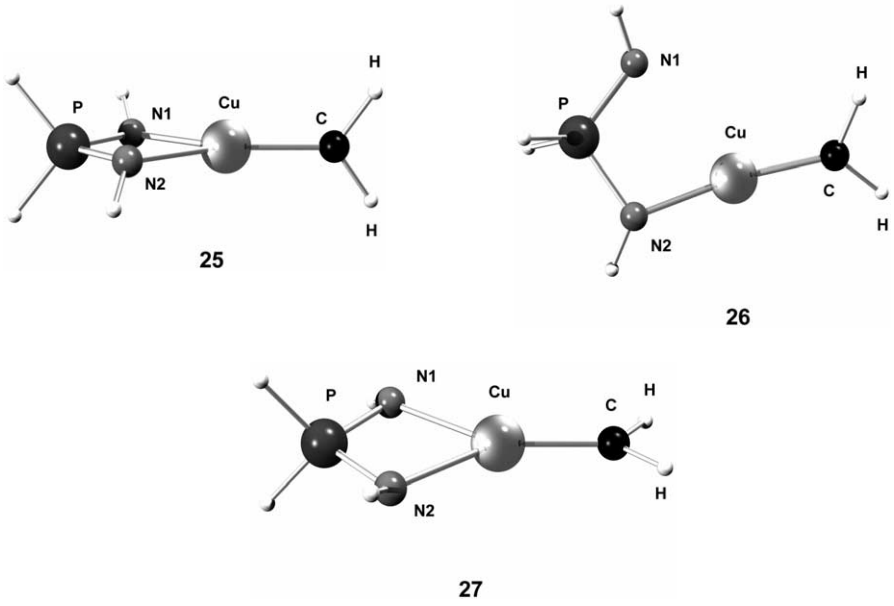

Fig. 18. Ball-and-stick models of the carbene complex **25**, the transition state for carbene rotation **26** and the C_2 symmetric stationary point **27**.

cyclopropanation is in accordance with the lowering of the activation barrier for vinyl alcohol compared to ethene (Table 6).

The electrophilic character of the carbene complex in the transition state **28** is reflected in the NBO net charge transfer of −0.14 of the ethene nucleophile to the carbene. In accordance with the formal oxidation of the copper(I) carbene **8** to the copper(III) complex **31**, the direction of the charge transfer changes in the course of the reaction. As expected, the charge transfer is even more pronounced in transition state **31** with its electron-rich vinyl alcohol as a nucleophile (Table 7).

Model complex **29** and transition state **30** could only be localized at the B3LYP/[SDD/6-31G(d)] level of theory. Upon B3LYP/6-31G(d) geometry-optimization of structure **29**, cupracyclobutane **31** is directly formed. Again, the importance of the basis set quality on copper is apparent.

The shallow nature of the reaction energy surface around the structures **29**–**32** makes these complexes very sensitive towards steric repulsion of the spectator ligand (Fig. 21). Cupracyclobutane model **31** undergoes extremely facile reductive elimination to formyl cyclopropane and the copper(I) fragment **32**. Thus, it is probable that cyclopropanation reactions with sterically demanding semicorrin, [4] bisoxazolylmethane [32] or iminophosphanamide [8,10] ligands result in the direct formation of cyclopropane derivatives without cupracyclobutane intermediates. Less electron-donating spectator ligands destabilize the oxidation state III of copper. Accordingly, a cationic copper carbene model complex was reported to prefer direct cyclopropanation in the gas phase, [14] avoiding the high oxidation state III on copper.

Steric shielding of the copper center will further increase the activation barrier for the reaction of copper carbenes with alkenes. The successful detection of carbene complex **4** in the presence of ethene underlines the role of sterically demanding spectator ligands. Even addition of an excess of styrene to a solution with a steady-state concentration of complex **4** does not result in an immediate disappearance of the violet color of the carbene complex, but in a slow fading of the color within few minutes [10,11a].

Table 5
Relevant bond lengths (Å) and bond angles (°) of the copper iminophosphanamide complexes **25**, **26** and **27** [B3LYP/{SDD/6-31G(d)}]

	25	**26**	**27**
Bond length			
d(Cu–N1)	2.031	2.570	2.090
d(Cu–N2)	2.031	1.875	2.090
d(Cu–C)	1.788	1.795	1.806
Bond angles			
α(N2–Cu–C)	141.9	169.2	143.2

3.6.9. Comparison with the Pfaltz model

The transition state **30** has essentially the same structure of the copper carbene alkene backbone as in the model put forward by the Pfaltz co-workers in order to rationalize the origin of the enantioselectivities obtained with their C_2-symmetric semicorrin system [4]. In their model, the orthogonal carbene and N_2Cu moieties of the disfavored transition state lead to a repulsive interaction of the alkoxy carbonyl substituent of the carbene with a sterically demanding substituent of

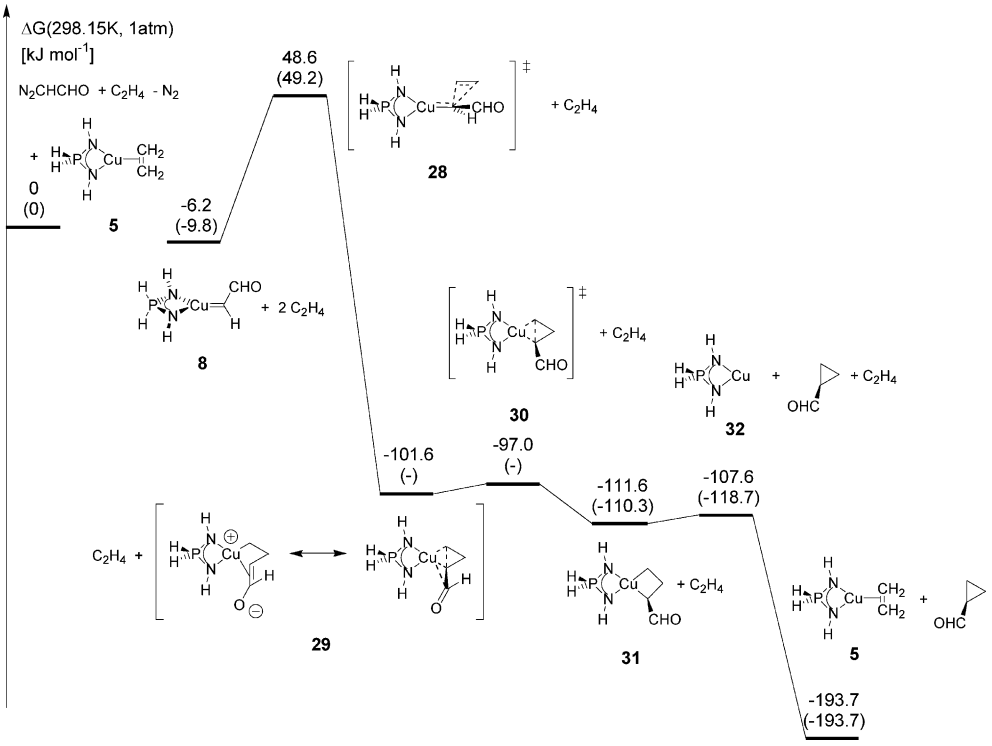

Fig. 19. Computed pathway of alkene cyclopropanation by copper(I) carbene model complex **8**. Gibbs free energies refer to B3LYP/SSD*+,6-311+G(2d,p)//B3LYP/SDD,6-31G(d) (in parentheses B3LYP/6-311+G(2d,p)//B3LYP/6-31G(d)).

the spectator ligand in one quadrant. In the model structures **29**–**31** (Fig. 21), the acyl group is indeed strongly bent towards the spectator ligand. Thus, a large energy difference of the diastereomeric transition states with chiral spectator ligands can be caused by the increasing steric repulsion of acyl and spectator ligand in the course of the C–C bond formation process.

3.6.10. Absolute carbene dissociation energies

The bond strengths of ethene, singlet formyl carbene and singlet methylene towards the copper iminophosphanamide fragment **32** in the model complexes **5**, **8** and **25** were computed (Table 8).

The ethene bond strengths to the uncharged copper model fragment are weaker than the previously computed bond strengths in $[Cu(C_2H_4)]^+$ of 184–238 kJ mol^{-1} [33]. In $[\{H_2C(CH{=}NMe)_2{-}\kappa^2N\}Cu(C_2H_4)]^+$, an ethene free dissociation energy of 143 kJ mol^{-1} has been computed [13]. The positive charge in these complexes significantly strengthens the ethene coordination to copper(I) fragments in the gas phase.

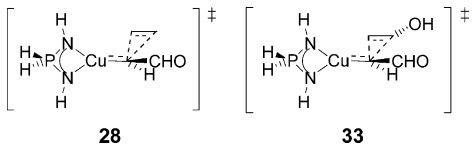

28 **33**

Fig. 20. Model transition states **28** and **33** for the reaction of the electrophilic copper(I) carbene complex **8** with ethene and vinyl alcohol.

The copper carbon double bond character in the copper carbenes **8** and **25** is reflected in high carbene bond strengths. A Gibbs free energy for carbene dissociation of 195.4 kJ mol^{-1} (187.9 kJ mol^{-1}) in model **8** clearly demonstrates that the generation of free carbenes from copper carbene complexes is no alternative mechanistic pathway in copper-catalyzed cyclopropanation. MP2 and CCSD(T) computations of CuCl Wanzlick–Arduengo carbene complexes revealed dis-

Table 6
Relevant bond lengths (Å) and bond angles (°) of the copper iminophosphanamide complexes **28**–**31** and **33** [B3LYP/{SDD/6-31G(d)}]

	28	**29**	**30**	**31**	**33**
Bond length					
d(Cu–N1)	2.030	2.163	2.106	2.027	2.094
d(Cu–N2)	1.976	1.992	2.028	2.023	2.034
d(Cu–C1)	2.852	2.618	2.624	2.690	2.894
d(Cu–C2)	1.796	2.217	2.105	1.984	1.841
d(Cu–C3)	2.796	2.201	2.073	1.951	2.966
d(C1–O)	1.220	1.214	1.214	1.219	1.223
d(C1–C2)	1.471	1.494	1.491	1.476	1.471
d(C2–C3)	2.226	1.635	1.777	2.196	2.269
d(C2–C4)	2.505	1.515	1.510	1.525	2.664
d(C3–C4)	1.359	1.488	1.489	1.512	1.361
Bond angles					
α(N2–Cu–C2)	143.5	133.6	122.2	108.5	149.0
α(N1–Cu–C3)	87.6	107.4	111.6	107.4	86.1
α(Cu–C2–C1)	121.3	87.4	92.2	101.0	121.4

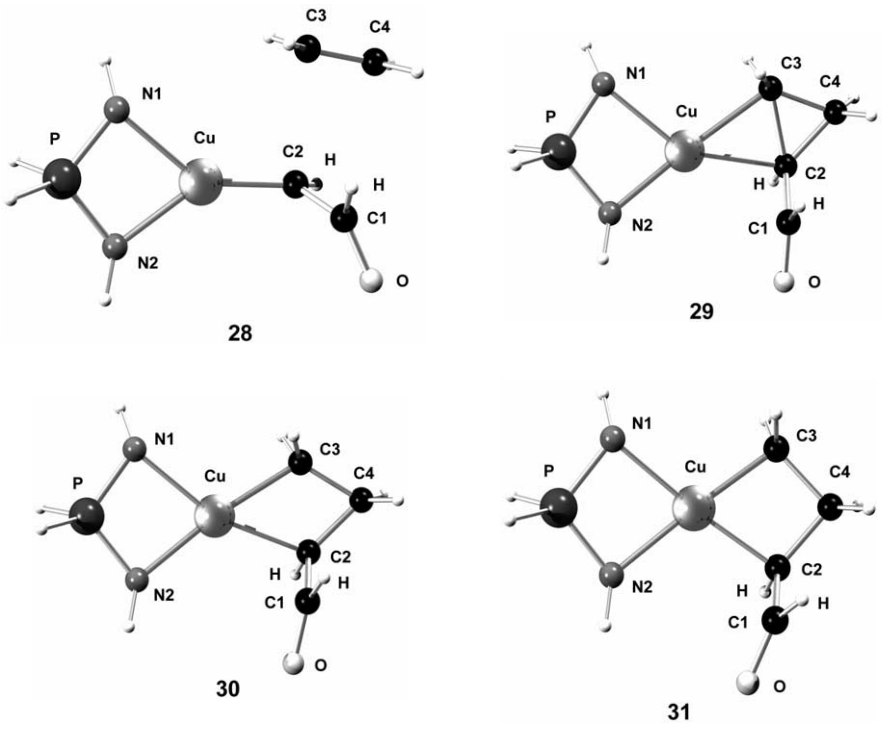

Fig. 21. Ball-and-stick models of the transition state for ethene cyclopropanation **28**, cyclopropanation intermediate **29**, transition state **30** and cupracyclobutane **31**.

sociation energies of 282 and 319 kJ mol^{-1}, [27] which are very similar to our D_e values of 257.9–312.4 kJ mol^{-1}.

In the cyclopropanation reaction of alkenes with copper carbenes, the alkene and the copper carbene double bond disappear and three strained carbon–carbon single bonds are formed. Though one bonding interaction is formally lost, the cyclopropanation reaction is exergonic due to the relative weakness of the copper–carbon double bond compared to carbon–carbon single bonds.

3.6.11. Comparison of cyclopropanation mechanisms via d^{10} transition metal carbene intermediates

Both for copper(I) and palladium(0) cyclopropanation catalysis, mechanistic insight is based upon experimental investigations and quantum-chemical model calculations [12–14,34]. Several similarities exist for the mechanism of the copper(I) and palladium(0) catalytic cycle. For both metals, the catalyst resting state is a d^{10} alkene complex and the reactive intermediate is a d^{10} carbene complex. The rate-determining step is the N_2 elimination from a κC-diazoalkane complex, respectively (Scheme 6).

Whereas copper(I) fragments bind stronger to electron-rich donor alkenes than to electron-deficient alkenes, the opposite is true for palladium(0) fragments. Thus, the palladium(0) cyclopropanation catalyst can be inhibited by maleic esters, [35] while the activity of copper(I) catalysts is insensitive towards such alkenes. In contrast to copper(I), palladium(0) binds stronger to

Table 7
NBO charges in ethene, **8**, **28**, **29**, **30**, **31**, vinyl alcohol and **33**.

	Cu	Carbene C	Alkene fragment
C_2H_4	–	–	0
8	0.99	−0.45	–
28	0.94	−0.47	0.14
29	0.85	−0.39	0.08
30	0.90	−0.39	0.02
31	1.05	−0.45	−0.14
C_2H_3OH	–	–	0
33	0.95	−0.49	0.16

Table 8
Electronic bond strengths corrected by zero point energies and free Gibbs energies of dissociation of C_2H_4, ^{1}CHCHO and $^1CH_2$ in kJ mol^{-1}

	D_e [a]	D_0 [b]	BDE [c]	$\Delta G_{298.15K}$
5→**32**+C_2H_4	140.2 (133.5)	131.8 (122.7)	134.0 (125.6)	86.1 (75.1)
8→ **32**+^{1}CHCHO	261.4 (257.9)	251.5 (246.6)	252.8 (248.0)	195.4 (187.9)
25→**32**+$^1CH_2$	312.4 (310.4)	291.9 (288.1)	296.9 (293.4)	251.4 (245.4)

All electron basis set energies in parentheses.
[a] Difference of total electronic energies.
[b] Including zero point vibrational energy correction.
[c] BDE = ΔH (298.15 K, 1 atm).

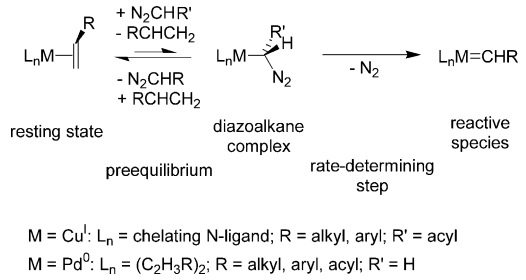

Scheme 6. Initializing mechanistic steps of alkene cyclopropanation by d^{10} metal fragments.

an acceptor-substituted alkene substrate than to chelating N-ligands [34,36]. As a consequence, chiral N-ligands induce high enantioselectivities in copper-catalyzed alkene cyclopropanation. Analogous ligands in palladium-catalyzed cyclopropanation lead to 0% ee, since alkene substrate ligands replace the nitrogen ligands in catalytically active palladium(0) species.

The most important difference between the copper(I) and the palladium(0) mechanism is the actual cyclopropanation sequence itself. The reactive copper(I)carbene intermediate undergoes a one-step, intermolecular, direct carbene fragment transfer reaction with the electron-rich alkene substrate to yield the cyclopropane product. The analogous palladium dialkene carbene intermediate, however, needs two steps: first, an intramolecular '*cis*-rearrangement' leads to the formation of a monoalkene pallada(II)cyclobutane. In the second step, a reductive elimination produces the cyclopropane product. The larger palladium atom and the lack of sterically demanding ancillary ligands enable the formation of transient pallada(II)cyclobutanes in this reaction.

4. Conclusions and summary

The generally observed preequilibrium in copper-catalyzed cyclopropanation of alkenes is due to an equilibrium of copper diazoalkane complexes, copper alkene complex and free diazoalkane and alkene ligand. Diazoalkane alkene ligand exchange pathways, which are faster than the N_2 loss and carbene complex formation, have been found computationally.

All computed intermediates and transition states of the catalytic cycle are closed-shell diamagnetic copper(I) or copper(III) complexes, in accordance with experimental data of observed or isolated intermediates. A high backbonding capability of the copper fragment is mandatory to stabilize the active copper carbene species. Electron-rich chelating nitrogen ligands indeed lead to a high backbonding capability of copper(I) and thus result in thermodynamically stable copper alkene complex resting states. Despite their thermodynamic stability, these alkene complexes are kinetically highly active. Cartesian coordinates for structures in Tables 9–11 can be obtained from authors.

The N_2 substitution in diazoalkanes by copper(I) fragments can be viewed as umpolung reaction. The nucleophilic diazo carbon is converted into an electrophilic center of a Fischer-type carbene complex.

5. Experimental

5.1. General

The starting material *t*-$Bu_2P[N(SiMe_3)]NH(SiMe_3)$ was synthesized according to a literature procedure [37]. Benzoquinone was sublimed prior to use. Deuterated solvents were dried and distilled prior to use.

5.2. Synthesis of maleic anhydride complex **9**

Under an argon atmosphere, ca. 2.5–3 ml of 1.6 M *n*-BuLi in hexane (4.5 mmol) was added to 1.2 g (3.75 mmol) *t*-$Bu_2P[N(SiMe_3)]NH(SiMe_3)$ in 10 ml of hexane. The solution was heated to reflux temperature for 1 min, then added to a suspension of 4.97 g (24 mmol) CuBr·SMe_2 in 10 ml of hexane at 195 K and stirred while warming to ambient temperature. A copper mirror on the wall of the glass can sometimes be formed. 0.4 g (4.1 mmol) maleic anhydride was added. After stirring for 90 min at ambient temperature, the suspension was filtered through Celite. The Celite was washed once with hexane. The solution was concentrated in vacuo. Yellow crystals precipitated. From the orange–yellow solution crude **9** was crystallized at −78°C. Recrystallization yielded 613 mg (68%), m.p.: 84 °C, 89−90 °C dec. ^{1}H-NMR (298 K, toluene-d_8, 300.13 MHz): δ 4.24 (s, $^1J_{CH} = 181$ Hz, =CH; 2H), 1.03 (d, $^3J_{PH} = 14$ Hz, $^1J_{CH} = 129$ Hz, $C(CH_3)_3$; 18H), 0.21 (s+sat., $^1J_{CH} = 120$ Hz, $Si(CH_3)_3$; 18H). $^{13}C\{^1H\}$-NMR (298 K, toluene-d_8, 75.47 MHz): δ 165.3 (s, CO), 70.9 (s, =CH), 37.7 (d, $^1J_{CP} = 60$ Hz, $C(CH_3)_3$), 27.7 (s, $C(CH_3)_3$), 5.63 (d, $^3J_{PC} = 3$ Hz, $Si(CH_3)_3$). VT $\{^1H\}$-NMR (toluene-d_8, 300.13 MHz): $C(CH_3)_3$, $T_c = (251 \pm 4.0)$ K, $k_c = 13.5$ Hz. VT $^{13}C\{^1H\}$-NMR (toluene-d_8, 75.47 MHz): $C(CH_3)_3$, $T_c = (259 \pm 4.0)$ K, $k_c = 39$ Hz; $C(CH_3)_3$, $T_c = (267.5 \pm 4.0)$ K, $k_c = 79$ Hz; temperature calibration by external MeOH. $^{29}Si\{^1H\}$-NMR DEPT (298 K, toluene-d_8, 59.63 MHz): δ −6.5 (d+sat., $^2J_{Psi} = 11$ Hz, $^1J_{CSi} = 43$ Hz). $^{31}P\{^1H\}$-NMR (298 K, toluene-d_8, 121.50 MHz): δ 75.9 (s). IR (KBr pellet, cm^{-1}): 2951 (s), 2900 (m), 1848 (w), 1834 (m), 1775 (s), 1570 (s), 1478 (m), 1395 (m), 1348 (s), 1250 (d), 1227 (m), 1105 (s), 1050 (w), 922 (w), 892 (m), 838 (vs), 759 (m), 699 (m), 670 (m), 643 (m), 625 (m), 481 (m). UV (pentane, nm): 207, 295. Calc. for $C_{18}H_{38}N_2CuO_3PSi_2$: C, 44.93; H, 7.96; N, 5.82; P, 6.44. Found: C, 44.93; H, 8.06; N, 6.05; P, 6.40%.

Table 9
Computed energies of the model compounds **5**–**22** at the B3LYP/[SDD+*/6-311+G(2d,p)]//B3LYP/[SDD/6-31G(d)] level of theory (a.u.)

	E[SDD/6-31G(d)]	Single-point electronic energy E[SDD/6-311+G(2d,p)]	Gibbs free energy correction	G[SDD/6-31G(d)]	G[SDD/6-311+G(2d,p)]
5	−729.220085	−729.345852	0.070664	−729.149421	−729.275188
6	−923.356235	−923.532889	0.166170	−923.190065	−923.366719
6‡	−923.344701	−923.523023	0.165398	−923.177691	−923.357625
7	−912.700690	−912.882129	0.058688	−912.642002	−912.823441
8a	−803.154874	−803.304120	0.046659	−803.108216	−803.257461
8b	−803.154152	−803.303643	0.046318	−803.107834	−803.257325
14	−1029.915298	−1030.139189	0.068792	−1029.846505	−1030.070397
14‡	−1029.897253	−1030.122181	0.067224	−1029.830029	−1030.054957
15	−1032.077722	−1032.297776	0.096703	−1031.981019	−1032.201073
15‡	−1032.060899	−1032.282258	0.094915	−1031.965984	−1032.187343
15b‡	−1032.057957	−1032.278494	0.096078	−1031.961879	−1032.182416
16	−954.594858	−954.795679	0.057047	−954.537811	−954.738632
17	−991.280046	−991.489861	0.104744	−991.175302	−991.385117
18	−991.265252	−991.477668	0.097972	−991.167280	−991.378708
19	−912.678412	−912.861212	0.052939	−912.625473	−912.808273
20	−912.683723	−912.868054	0.055089	−912.628634	−912.812965
21	−912.668940	−912.853787	0.055037	−912.613903	−912.798750
22	−912.676743	−912.863092	0.052302	−912.624441	−912.810790
23	−912.660036	−912.846088	0.051591	−912.608446	−912.794497
24	−803.151088	−803.301750	0.050504	−803.100583	−803.251246
25	−689.832180	−689.942308	0.042476	−689.789704	−689.899832
26	−689.815927	−689.926191	0.040048	−689.775879	−689.886143
27	−689.811591	−689.922081	0.040708	−689.770883	−689.881373
28	−881.742405	−881.920198	0.095720	−881.646685	−881.824478
29	−881.807990	−881.982177	0.100561	−881.707430	−881.881616
30	−881.807290	−881.981713	0.101803	−881.705487	−881.879910
31	−881.814054	−881.988790	0.103322	−881.710732	−881.885468
32	−650.578891	−650.674917	0.020366	−650.558525	−650.654551
33	−956.962433	−957.175485	0.099159	−956.863274	−957.076326

5.3. Synthesis of benzoquinone complex **10**

Under an argon atmosphere ca. 2.5–3 ml of 1.6 M *n*-BuLi in hexane (ca. 4.5 mmol) was added to 1.2 g (18.0 mmol) *t*-$Bu_2P[N(SiMe_3)]NH(SiMe_3)$ in 10 ml of hexane. The solution was heated to reflux temperature for 1 min, then added to a suspension of 1.0 g (4.9 mmol) CuBr·SMe_2 in 10 ml of hexane at 195 K and stirred while warming to ambient temperature. 0.44 g (4.1 mmol) 1,4-benzoquinone was added. The suspension was filtered through Celite. From the red–orange solution crude **10** was isolated by removing the solvent in vacuo. Excess of 1,4-benzoquinone was removed at 10^{-3} mbar. After dissolving **10** in hexane and filtration, attempts to crystallize **10** failed. The metallic golden material thus has not yet been purified. ^{1}H-NMR (298 K, toluene-d_8, 300.13 MHz): δ 5.34 (br s, =CH; 4H), 1.07 (d, $^3J_{PH} = 14$ Hz, $^1J_{CH} = 126$ Hz, $C(CH_3)_3$; 18H), 0.23 (s+sat., $^1J_{CH} = 118$ Hz, $Si(CH_3)_3$; 18H). ^{1}H-NMR (213 K, toluene-d_8, 300.13 MHz): δ 5.85 (s, =CH; 2H), 4.29 (s, $^1J_{CH} = 181$ Hz, CuCH; 2H), 1.05 (d, $C(CH_3)_3$; 18H), 0.29 (s, $Si(CH_3)_3$; 18H). $^{13}C\{^1H\}$-NMR (298 K, toluene-d_8, 75.47 MHz): δ 186.3 (s, CO), 37.9 (d, $^1J_{CP} = 60$ Hz, $C(CH_3)_3$), 28.0 (s, $C(CH_3)_3$), 5.7 (s, $Si(CH_3)_3$). $^{13}C\{^1H\}$-NMR (213 K, toluene-d_8, 75.47 MHz): δ 186.5 (s, CO), 138.0 (s, =CH), 78.4 (s, CuCH), 38.0 (d, $^1J_{CP} = 59$ Hz, $C(CH_3)_3$), 37.0 (d, $^1J_{CP} = 62$ Hz, $C(CH_3)_3$), 28.1 (s, $C(CH_3)_3$), 26.8 (s, $C(CH_3)_3$), 5.5 (d, $^3J_{PC} = 2$ Hz, $^1J_{CH} = 57$ Hz, $Si(CH_3)_3$). $^{29}Si\{^1H\}$-NMR DEPT (298 K, toluene-d_8, 59.63 MHz): δ −8.2 (d+sat., $^2J_{Psi} = 12$ Hz, $^1J_{CSi} = 57$ Hz). $^{31}P\{^1H\}$-NMR (298 K, toluene-d_8, 121.50 MHz): δ 73.6 (s). VT $\{^1H\}$-NMR (toluene-d_8, 300.13 MHz): C*H*, $T_c = (267 \pm 4.0)$ K, $k_c = 466$ Hz. VT $^{13}C\{^1H\}$-NMR (toluene-d_8, 75.47 MHz): $C(CH_3)_3$, $T_c = (241 \pm 4.0)$ K, $k_c = 71$ Hz; $C(CH_3)_3$, $T_c = (244 \pm 4.0)$ K, $k_c = 102$ Hz; temperature calibration by external MeOH.

5.4. Synthesis of styrene complex **11**

Under an argon atmosphere, 8 ml of 1.6 M *n*-BuLi in hexane (15 mmol) was added to 3.2 g (10 mmol) *t*-$Bu_2P[N(SiMe_3)]NH(SiMe_3)$ in ca. 15 ml of hexane. The solution was heated to reflux temperature for 1 min, then added to a suspension of 2.6 g (13 mmol) CuBr·SMe_2 in 20 ml of hexane at 195 K and stirred while warming to ambient temperature. Twelve milliliter of styrene was added to the black suspension. The suspension was filtered through Celite. Only a part of the black colloidal copper, presumably copper hydrides or copper

Table 10
Computed energies of the model compounds **5**–**23** at the B3LYP/6-311+G(2d,p)//B3LYP/6-31G(d) level of theory (a.u.)

	E[6-31G(d)]	Single-point electronic energy E[6-311+G(2d,p)]	Gibbs free energy correction	G[6-31G(d)]	G[6-311+G(2d,p)]
5	−2172.168525	−2172.492752	0.071831	−2172.096694	−2172.420921
6	−2366.313941	−2366.680111	0.167350	−2366.146591	−2366.512761
6‡	−2366.299621	−2366.669244	0.166903	−2366.132717	−2366.502341
7	−2355.665586	−2356.029340	0.060435	−2355.605151	−2355.968905
8a	−2246.108291	−2246.452242	0.047645	−2246.060645	−2246.404597
8b	−2246.109087	−2246.452271	0.047962	−2246.061125	−2246.404309
14	−2472.876137	−2473.287436	0.069231	−2472.806906	−2473.218205
14‡	−2472.856022	−2473.270311	0.067828	−2472.788194	−2473.202483
15	−2475.036785	−2475.445678	0.096892	−2474.939892	−2475.348786
15‡	−2475.017998	−2475.430466	0.095472	−2474.922526	−2475.334994
15b‡	−2475.019872	−2475.426039	0.096787	−2474.923085	−2475.329252
16	−2397.555270	−2397.943746	0.057046	−2397.498223	−2397.886700
17	−2434.238881	−2434.639495	0.104293	−2434.134587	−2434.535202
18	−2434.216553	−2434.620870	0.102687	−2434.113866	−2434.518183
19	−2355.616332	−2355.995740	0.056515	−2355.559818	−2355.939225
20	−2355.636412	−2356.015009	0.056611	−2355.579801	−2355.958398
21	−2355.622951	−2356.000990	0.056992	−2355.565959	−2355.943998
22	−2355.626014	−2356.004593	0.055917	−2355.570097	−2355.948676
23	−2355.607988	−2355.993496	0.053069	−2355.554919	−2355.940427
24	−2246.116629	−2246.449552	0.051474	−2246.065155	−2246.398078
25	−2132.781499	−2133.090981	0.043516	−2132.737983	−2133.047465
26	−2132.757744	−2133.073957	0.040529	−2132.717214	−2133.033332
27	−2132.754748	−2133.071474	0.042178	−2132.712570	−2133.029296
28	−2324.691782	−2325.067996	0.098039	−2324.593742	−2324.969957
31	−2324.779338	−2325.135827	0.105111	−2324.674227	−2325.030716
32	−2093.485775	−2093.824366	0.019871	−2093.465903	−2093.804495
33	−2399.912595	−2400.323839	0.100309	−2399.812287	−2400.223530
C_2H_3OH	−153.802228	−153.867075	0.031538	−153.770690	−153.835537
N_2	−109.524129	−109.562947	−0.012851	−109.536980	−109.575798
C_2H_4	−78.587458	−78.617536	0.029696	−78.557762	−78.587840
N_2CHCHO	−262.071651	−262.159010	0.015421	−262.056230	−262.143589
C_3H_5CHO	−231.218147	−231.292916	0.063504	−231.154644	−231.229412
CHCHO	−152.474031	−152.529641	0.005923	−152.468108	−152.528518
CH_2	−39.128249	−39.148393	−0.001123	−39.129372	−39.149516
$C_4H_2O_3$	−379.289544	−379.414165	0.026816	−379.262729	−379.387349
C_7H_{10}	−272.727426	−272.805262	0.125138	−272.602289	−272.680124
$C_6H_4O_2$	−381.451687	−381.572242	0.056158	−381.395529	−381.516084
$C_2(CHO)_2$	−303.964053	−304.066219	0.016626	−303.947427	−304.049593

clusters, were removed. The black solution was concentrated in vacuo at 10^{-3} mbar. Excess of styrene was removed within 12 h at 10^{-5} mbar. The black oil crystallized within several days at ambient temperatures. Small colorless crystals embedded in a black matrix were isolated. Further attempts of filtration and crystallization failed. Complex **11** is not available in analytically pure form. ^{1}H-NMR (298 K, toluene-d_8, 300.13 MHz): δ 7.25 (d, $^3J_{HH} = 8$ Hz, *o*-CH; 2H), 7.02 ('t', $^3J_{HH} = 7.5$ Hz, *m*-CH; 2H), 6.96 (d, $^3J_{HH} = 7$ Hz, *p*-CH; 1H), 5.02 (dd, $^3J_{HH} = 9.2$ Hz and 14.6, =CH *gem*; 1H), 3.92 (d, $^3J_{HH} = 14.6$, =CH *cis*; 1H), 3.59 (d, $^3J_{HH} = 9.2$ Hz, =CH *trans*; 1H), 1.17 (d, $^3J_{PH} = 14.5$ Hz, $^1J_{CH} = 128$ Hz, C(CH_3)$_3$; 18H), 0.11 (s+sat., $^1J_{CH} = 110$ Hz, Si(CH_3)$_3$; 18H). ^{13}C{^{1}H}-NMR (298 K, toluene-d_8, 75.47 MHz): δ 139.7 (s, *ipso*-C), 128.8 (s), 127.5 (s, *p*-CH), 12 6.3 (s), 91.0 (s, PhC), 68.2 (s, CH_2), 37.4 (d, $^1J_{CP} = 64$ Hz, $C(CH_3)_3$), 28.1 (d, $^2J_{CP} = 2$ Hz, C(CH_3)$_3$), 5.5 (d+sat., $^1J_{SiC} = 57$ Hz, $^3J_{PC} = 2$ Hz, Si(CH_3)$_3$). ^{29}Si{^{1}H}-NMR DEPT (298 K, toluene-d_8, 59.63 MHz): δ −14.5 (d, $^2J_{Psi} = 15.5$ Hz). ^{31}P{^{1}H}-NMR (298 K, toluene-d_8, 121.50 MHz): δ 61.7 (s+sat., $^1J_{CP} = 64$ Hz, $^2J_{Psi} = 14$ Hz). VT ^{13}C{^{1}H}-NMR (toluene-d_8, 75.47 MHz): C(CH_3)$_3$, $T_c = (181.5 \pm 4.0)$ K, $k_c = 42$ Hz; Si(CH_3)$_3$, $T_c = (185.5 \pm 4.0)$ K, $k_c = 61$ Hz; temperature calibration by external MeOH.

5.5. Synthesis of dimethyl butynedioate complex *12*

Under an argon atmosphere, 262 mg dimethyl butynedioate (1.79 mmol) and 752 mg (1.82 mg) ethene complex **1** were dissolved in 5 ml Et_2O. Gas evolution occurred. Upon standing overnight at 223 K, yellow crystals precipitated. The crystals were dissolved in Et_2O/THF and filtered through Celite. The solution was concentrated in vacuo and cooled to 223 K. Yellow

Table 11
Zero point energies and *H* corrections (a.u.)

	B3LYP/[SDD/6-31G(d)]		B3LYP/6-31G(d)	
	ZPE	*H* correction	ZPE	*H* correction
CH_2	0.016586	0.020368	0.016586	0.020368
CHCHO	0.030043	0.034523	0.030039	0.034523
C_2H_4	0.051126	0.055212	0.051126	0.055212
C_7H_{10}	0.153656	0.159801	0.153656	0.159801
$C_4H_2O_3$	0.055890	0.062019	0.055890	0.062019
$C_6H_4O_2$	0.085366	0.092543	0.085366	0.092543
$C_2(CHO)_2$	0.047306	0.054611	0.047306	0.054611
5	0.103616	0.113294	0.104684	0.114029
6	0.204834	0.217622	0.205844	0.218313
8	0.082973	0.093535	0.083702	0.094098
14	0.107585	0.120081	0.108255	0.120623
15	0.136918	0.150576	0.137529	0.151081
16	0.098683	0.112502	0.099230	0.112918
25	0.073581	0.082021	0.074429	0.082667
32	0.049184	0.055731	0.049342	0.055817

crystals of **12** (220 mg, 86% yield) were obtained. M.p.: 101–102 °C (dec., turns red). ^{1}H-NMR (298 K, C_6D_6, 300.13 MHz): δ 3.40 (s, OMe), 1.15 (d+sat., $^3J_{PH} = 14$ Hz, $^1J_{CH} = 128$ Hz, C(CH_3)$_3$; 18H), 0.17 (s+sat., $^1J_{CH} = 117$ Hz, Si(CH_3)$_3$; 18H). ^{13}C{^{1}H}-NMR (298 K, C_6D_6, 75.47 MHz): δ 157.2 (s, CO), 100.3 (s, ≡C), 52.6 (s, OMe), 37.8 (d, $^1J_{CP} = 61$ Hz, *C*(CH$_3$)$_3$), 27.7 (d, $^2J_{CP} = 2$ Hz, C(*C*H$_3$)$_3$), 4.9 (d+sat., $^1J_{SiC} = 58$ Hz, $^3J_{PC} = 2$ Hz, Si(*C*H$_3$)$_3$). ^{29}Si{^{1}H}-NMR DEPT (298 K, C_6D_6, 59.63 MHz): δ −7.9 (d+sat., $^2J_{Psi} = 10$ Hz). ^{31}P{^{1}H}-NMR (298 K, C_6D_6, 121.50 MHz): δ 73.5 (s, $^1J_{CP} = 64$ Hz). IR (KBr pellet, cm^{-1}): 3000 (w), 2951 (s), 2900 (m), 1949 (m), 1920 (m), 1732 (s), 1714 (s), 1478 (w), 1428 (m), 1397 (w), 1347 (m), 1248 (vs), 1159 (m), 1123 (s), 1037 (m), 923 (w), 836 (s), 759 (m), 701 (m), 667 (w), 644 (m), 625 (w), 521 (w), 480 (w). UV (pentane): 207, (241 sh), 296. FABMS (*m*-nitrobenzyl alcohol): *m*/*z* (%) = 524.2 (21.7) [M$^+$]. Calc. for $C_{20}H_{42}N_2CuO_4PSi_2$: C, 45.73; H, 8.06; N, 5.33; P, 5.90. Found: C, 45.99; H, 8.17; N, 5.62; P, 5.74%.

6. Supplementary material

Crystallographic data for the structural analysis have been deposited with the Cambridge Crystallographic data Centre, CCDC no. 214068 for compound **9** and no. 214069 for compound **12**. Copies of this information may be obtained free of charge from The Director, CCDC, 12 Union Road, Cambridge CB2 1EZ, UK (Fax: +44-1223-336033; e-mail deposit@ccdc.cam.ac.uk or www: http://ccdc.cam.ac.uk.

Acknowledgements

A doctoral fellowship for B.F.S. from the *Fonds der Chemischen Industrie* is gratefully acknowledged.

References

[1] (a) W. Kirmse, Angew. Chem. 115 (2003) 1120 (Angew. Chem. Int. Ed. 42 (2003) 1088);
(b) M.P. Doyle, M.A. McKervey, T. Ye, Modern Catalytic Methods for Organic Synthesis with Diazo Compounds, Wiley, New York, 1998.
[2] (a) H. Nozaki, S. Moriuti, H. Takaya, R. Noyori, Tetrahedron Lett. (1966) 5239;
(b) H. Nozaki, H. Takaya, S. Moriuti, R. Noyori, Tetrahedron 24 (1968) 3655.
[3] T. Aratani, Pure Appl. Chem. 57 (1985) 1839.
[4] H. Fritschi, U. Leutenegger, A. Pfaltz, Helv. Chim. Acta 71 (1988) 1553.
[5] (a) M. Mar Díaz-Requejo, M.C. Nicasio, P.J. Pérez, Organometallics 17 (1998) 3051;
(b) M. Mar Díaz-Requejo, T.R. Belderrain, M.C. Nicasio, F. Prieto, P.J. Pérez, Organometallics 18 (1999) 2601.
[6] P.J. Pérez, M. Brookhart, J.L. Templeton, Organometallics 12 (1993) 261.
[7] (a) R.W. Quan, Z. Li, E.N. Jacobsen, J. Am. Chem. Soc. 11 (1996) 8156;
(b) M.M.-C. Lo, G.C. Fu, J. Am. Chem. Soc. 120 (1998) 10270;
(c) L. Cavallo, M.E. Cucciolito, A. De Martino, F. Giordano, I. Orabona, A. Vitagliano, Chem. Eur. J. 6 (2000) 1127.
[8] B.F. Straub, F. Eisenträger, P. Hofmann, Chem. Commun. (1999) 2507.
[9] B.F. Straub, F. Rominger, P. Hofmann, Organometallics 19 (2000) 4305.
[10] B.F. Straub, P. Hofmann, Angew. Chem. 113 (2001) 1328 (Angew. Chem. Int. Ed. 40 (2001) 1288).
[11] (a) Bernd F. Straub, Dissertation, Ruprecht-Karls Universität, Heidelberg, (2000);
(b) B.F. Straub, F. Rominger, P. Hofmann, Unraveling the Mechanism of Copper-Catalyzed Cyclopropanation, IV Symposium 'Selective Reactions of Metal-Activated Molecules', Würzburg, September 2000.
[12] M. Bühl, F. Terstegen, F. Löffler, B. Meynhardt, S. Kierse, M. Müller, C. Näther, U. Lüning, Eur. J. Org. Chem. (2001) 2151.
[13] J.M. Fraile, J.I. Garcia, V. Martinez-Merino, J.A. Mayoral, L. Salvatella, J. Am. Chem. Soc. 123 (2001) 7616.
[14] T. Rasmussen, J.F. Jensen, N. Ostergaard, D. Tanner, T. Ziegler, P.-O. Norrby, Chem. Eur. J. 8 (2002) 177.
[15] (a) A.D. Becke, J. Chem. Phys. 98 (1993) 5648;
(b) S.H. Volko, L. Wilk, M. Nusair, Can. J. Phys. 58 (1980) 1200;
(c) C. Lee, W. Yang, R.G. Parr, Phys. Rev. B 37 (1988) 785.
[16] M.J. Frisch, G.W. Trucks, H.B. Schlegel, G.E. Scuseria, M.A. Robb, J.R. Cheeseman, V.G. Zakrzewski, J.A. Montgomery Jr., R.E. Stratman, J.C. Burant, S. Dapprich, J.M. Millam, A.D. Daniels, K.N. Kudin, M.C. Strain, O. Farkas, J. Tomasi, V. Barone, M. Cossi, R. Cammi, B. Mennucci, C. Pomelli, C. Adamo, S. Clifford, J. Ochterski, G.A. Petersson, P.Y. Ayala, Q. Cui, K. Morokuma, D.K. Malick, A.D. Rabuck, K. Raghavachari, J.B. Foresman, J. Cioslowski, J.V. Ortiz, B.B. Stefanov, G. Liu, A. Liashenko, P. Piskorz, I. Komaromi, R. Gomperts, R.L. Martin, D.J. Fox, T. Keith, M.A. Al-Laham, C.Y. Peng, A. Nanayakkara, C. Gonzalez, M. Challacombe, P.M.W. Gill, B. Johnson, W. Cheng, M.W. Wong, J.L. Andres, C. Gonzalez, M.

Head-Gordon, E.S. Replogle, J.A. Pople, Gaussian, Inc., Pittsburgh PA, 1998.
[17] M. Dolg, U. Wedig, H. Stoll, H. Preuss, J. Chem. Phys. 86 (1987) 866.
[18] (a) W.J. Hehre, R.J. Ditchfield, A. Pople, J. Chem. Phys. 56 (1972) 2257;
(b) P.C. Hariharan, J.A. Pople, Theor. Chem. Acta 28 (1973) 213;
(c) M.J. Frisch, J.A. Pople, J.S. Binkley, J. Chem. Phys. 80 (1984) 3265;
(d) T. Clark, J. Chandrasekhar, G.W. Spitznagel, P.V.R. Schleyer, J. Comp. Chem. 4 (1983) 294.
[19] P. Pyykkö, N. Runeberg, F. Mendizabal, Chem. Eur. J. 3 (1997) 1451.
[20] R. Krishnan, J.S. Binkley, R. Seeger, J.A. Pople, J. Chem. Phys. 72 (1980) 650.
[21] E.D. Glendening, A.E. Reed, J.E. Carpenter, F. Weinhold, NBO Version 3.1.
[22] P. Pyykkö, Chem. Rev. 88 (1988) 563.
[23] (a) B. Lenders, W. Kläui, M. Irmler, G. Meyer, J. Chem. Soc. Dalton Trans. (1990) 2069;
(b) W. Kläui, B. Lenders, B. Hessner, K. Evertz, Organometallics 7 (1988) 1357.
[24] J. Green, E. Sinn, S. Woodward, R. Butcher, Polyhedron 12 (1993) 991.
[25] D.B. Llevellynn, D. Adamson, B.A. Arndtsen, Org. Lett. 2 (2000) 4165.
[26] (a) A.J. Arduengo, III, H.V.R. Dias, J.C. Calabrese, F. Davidson, Organometallics 12 (1993) 3405;
(b) H.G. Raubenheimer, S. Cronje, P.J. Olivier, J. Chem. Soc. Dalton Trans. (1995) 313;
(c) H.G. Raubenheimer, S. Cronje, P.H. van Rooyen, P.J. Olivier, J.G. Toerien, Angew. Chem. 106 (1994) 687 (Angew. Chem. Int. Ed. Engl. 33 (1994) 672).
[27] C. Boehme, G. Frenking, Organometallics 17 (1998) 5801.
[28] K. Ackermann, P. Hofmann, F.H. Köhler, H. Kratzer, H. Krist, K. Öfele, H.R. Schmidt, Z. Naturforsch. 38b (1983) 1313.
[29] E.O. Fischer, A. Maasböl, Angew. Chem. 76 (1964) 645 (Angew. Chem. Int. Ed. Engl. 3 (1964) 580).
[30] K.M. Gillespie, E.J. Crust, R.J. Deeth, P. Scott, Chem. Commun. (2001) 785.
[31] P. Brandt, M.J. Södergren, P.G. Andersson, P.-O. Norrby, J. Am. Chem. Soc. 122 (2000) 8013.
[32] (a) R.E. Löwenthal, A. Abiko, S. Masamune, Tetrahedron Lett. 31 (1990) 6005;
(b) D.A. Evans, K.A. Woerpel, M.M. Hinman, M.M. Faul, J. Am. Chem. Soc. 113 (1991) 726;
(c) R.E. Löwenthal, S. Masamune, Tetrahedron Lett. 32 (1991) 7373.
[33] (a) M. Böhme, T. Wagener, G. Frenking, J. Organomet. Chem. 520 (1996) 31;
(b) R.H. Herwig, W. Koch, D. Schröder, H. Schwarz, J. Hrusák, P. Schwertfeger, J. Phys. Chem. A 100 (1996) 12253.
[34] B.F. Straub, J. Am. Chem. Soc. 124 (2002) 14195.
[35] A.J. Anciaux, A.J. Hubert, A.F. Noels, N. Petiniot, P.J. Teyssié, Org. Chem. 45 (1980) 695.
[36] S.E. Denmark, R.A. Stavenger, A.-M. Faucher, J.P. Edwards, J. Org. Chem. 62 (1997) 3375.
[37] O.J. Scherer, G. Schieder, Chem. Ber. 101 (1968) 4184.